This is to certify that the
thesis entitled

PRELIMINARY DESIGN CONSIDERATIONS FOR
INTEGRATING A COMPOSITE IMPELLER IN A PERMANENT
MAGNET BRUSHLESS MOTOR

presented by

Mark Hubert Mouland

has been accepted towards fulfillment
of the requirements for the

M.S. degree in Mechanical Engineering

Major Professor's Signature

04/16/07

Date

PRELIMINARY DESIGN CONSIDERATIONS FOR INTEGRATING A COMPOSITE IMPELLER IN A PERMANENT MAGNET BRUSHLESS MOTOR

By

Mark Hubert Mouland

A THESIS

Submitted to
Michigan State University
in partial fulfillment of the requirement
for the degree of

MASTER OF SCIENCE

MECHANICAL ENGINEERING

2007

ABSTRACT

PRELIMINARY DESIGN CONSIDERATIONS FOR
INTEGRATING A COMPOSITE IMPELLER IN A PERMANENT
MAGNET BRUSHLESS MOTOR

By

MARK HUBERT MOULAND

Utilizing water as a refrigerant in an air conditioning device is a complex problem that requires various innovative ideas in order to create a suitable compressor that can successfully obtain the extremely high compression ratios required. This compressor requires multiple stages of impellers, which in order to withstand the high forces must be a wound composite created on a winding machine.

The largest challenge is getting the impellers to spin at the extremely high speed necessary. It is proposed using an innovative design in which the entire impeller acts as the shaft of a permanent magnet brushless motor. By placing magnets around the circumference of the shroud, or integrating them in the shroud itself, the entire impeller can act as one large shaft in the center of a motor device.

This thesis aims to look at the background research required to create the motor for such a device. Included are discussions on basic refrigeration cycles, information regarding the composite impeller, an overview of magnetics, as well as a numerous equations, and data regarding overall permanent magnet motor design.

All of these data are subsequently integrated together in order to propose numerous designs for a motor solution. These designs are accompanied by graphs and charts to outline various trends present using multiple design parameters. The data are then used with a weighted design matrix in order to select a preliminary design solution.

TABLE OF CONTENTS

LIST OF TABLES

LIST OF FIGURES

NOMENCLATURE

A_s	*Area of the Stator*
A_{slot}	*Area of the Windable Slot*
B_g	*Air-gap Flux Density*
B_r	*Residual Induction*
B_{sy}	*Stator Yoke Flux Density*
B_t	*Tooth Flux Density*
C_Φ	*Flux Concentration Factor*
c_u	*Tangential Component of Fluid Flow*
D_{wire}	*Diameter of the Wire*
d_s	*Windable Slot Depth*
d_{s1}	*Windable Slot Depth inner Diameter*
d_{s2}	*Windable Slot Depth outer Diameter*
d_{sh}	*Shoe Tip Depth*
d_t	*Shoe Taper Depth*
eb	*back emf*
e	*Shaft Energy*
f_e	*Electrical Frequency*
f_m	*Mechanical Frequency*
g	*Air-gap length*
g_{slot}	*Air-gap length in the Slot Opening*
H	*Magnetic Field Intensity*

i *current*

K_l *Leakage Factor*

K_m *Motor Constant*

K_r *Reluctance Factor*

K_{sl} *Slot Correction Factor*

K_{st} *Lamination Stacking Factor*

K_{wb} *Bare Wire Slot Fill Factor*

l_m *Length of the Magnet (radial direction)*

l_{st} *Length of the stator (motor axial length)*

M_{magnet} *Total mass of the magnets in the motor*

M_{stator} *Total mass of the stator*

M_{total} *Total mass of the wires, magnets, and stator*

M_{wire} *Total mass of the wire windings for all phases*

N *Number of wire turns*

N_m *Number of Magnet Poles*

N_s *Number of Stator Teeth*

N_{sm} *Nominal Coil Span*

P *Power*

P_c *Permeance Coefficient*

P_e *Eddy Current Losses*

P_{slot} *Power losses in slot wiring (I^2R losses)*

P_{stage} *Power required to spin impeller*

R_m *Radius to outer magnet edge*

R_{ro} *Radius to rotor outer edge*

R_{slot} *Slot Resistance*

T *Torque*

u *Tangential Velocity of Impeller*

w_{s1} *Width of the slot at the bottom*

w_{s2} *Width of the slot at the top*

w_{sb} *Bottom Slot Width*

w_{so} *Slot Opening Width*

w_{sy} *Width of the Stator Yoke*

w_{tb} *Stator Tooth Width*

θ_m *Mechanical Position*

θ_e *Electrical Position*

θ_s *Angular Tooth width at air \-gap*

θ_t *Angular Slot Pitch*

μ_r *Recoil Permeability*

ρ *Resistivity of the wire*

ρ_{magnet} *Magnet Material Density*

ρ_{stator} *Stator Material Density*

ρ_{wire} *Wire Material Density*

Φ_t *Tooth Flux*

Φ_{total} *Total Stator Flux*

ω_m *Angular Speed*

INTRODUCTION

The goal of this thesis is to design a motor drive system for a compressor in a water as a refrigerant air conditioning unit. Instead of having an impeller in the compressor driven on a shaft, the instead goal is to make the entire impeller the "shaft" of an electric motor. This means that magnets are on the circumference of the impeller and are driven by a stator, which surrounds the impeller.

The design of a brushless permanent magnet motor to drive this system is a complex process that integrates numerous disciplines in order to obtain a suitable design. Overall, this thesis aims to be an introductory paper into this design methodology for creating a motor, as well as calculating and choosing possible solutions. This design can be divided into a few major challenges: (1) Determining the magnetic materials to be used in the impeller and their integration into the impeller, (2) Designing a motor for the selected magnetic material that achieves the desired combination of torque and rotational speed, and (3) Comparing numerous design parameters and seeing how they affect the overall efficiency, mass and motor constant.

A simple background in some engineering aspects that are necessary to fully understand the problem will first be discussed. These include a basic look at the refrigeration cycle and the challenges behind water as a coolant. A few basics about magnets are also covered. This includes choices of magnet to be used in the design and also different arrangement and array types for the magnets. This includes Halbach arrays as well as their advantages and disadvantages. Next, the composite impeller is introduced, explaining how it is created. This particular discussion includes how the

outer shroud of the impeller can be potentially magnetized as an alternative to the traditional method of attaching them onto the rotor.

Thereafter, relevant basic equations regarding the design of electric motors are presented. This covers simple winding theory, as well as pole design criteria, which includes determining the back electromotive force (emf) and air-gap flux necessary to obtain a given rotational speed. These equations are used with numerous simplifying assumptions to provide a simple design procedure that is followed in an excel spreadsheet.

Lastly, this thesis combines the above backgrounds, into preliminary design considerations for an electric motor that can drive the composite impeller. This is accomplished using data previously regarding the compressor specifics. The values for impeller sizes, power, and speed are all obtained through previous work. Thus, this thesis only focuses on the design of the innovative motor drive system. The goal is to use all of the information acquired in research to obtain a functional design that address all of the problems and constraints the compressor will face. Upon completion of this optimization, the final motor design for each of the compressor stages will be presented, as well as a general methodology to be used. These calculations will be supported with numerous charts and graphs that show key trends to be utilized in the future.

Although this paper's key considerations are for the applications relating to water as a coolant, it should be noted that a magnetically driven impeller has wide range applications in the design of ducted fans and even in turbines and propulsion devices suitable for use in unmanned, aerial vehicles.

BACKGROUND

Water as a Refrigerant:

Refrigerants have been a major environmental issue, most particularly in the past decade. Although the magnitude of the problem was unknown before, it is now widely known that many refrigerants actively contribute to the depletion of the ozone layer, as well as help promote global warming.

Older refrigerants such as R-12 had high ozone depletion potentials (ODP) and also high Global Warming Potentials (GWP). These have been replaced by safer alternatives, such as R134a (zero ODP) and R22. However, both of these still promote global warming.

Thus, it is important that alternative refrigerants are created. Water is one of the best choices as a refrigerant that could replace both of these.

Aside from being much safer for the environment, water has been shown to even save up to 30% on energy savings. [9] Thus, with the current energy crisis in the United States, water would lessen our dependence on foreign oil. In California alone, if 5% of all air conditioner units were water based, this would yield energy savings of 405 MW a year, out of 27,000 MW used for Air Conditioning. [2]

A basic ideal refrigeration cycle is fairly simple to understand and consists of four major parts. The compressor is a unit that adds enthalpy to the fluid flow and is the driving force behind the cycle by increasing the pressure and temperature of the coolant. Next comes the condenser, which takes superheated vapor from the outlet of the compressor and condenses it in a constant pressure process to a saturated liquid. This is

the process that rejects heat into the surroundings. The expansion valves expand this saturated liquid, causing a very quick drop in pressure at constant entropy. Finally, the evaporator is what takes heat in from the surroundings and creates the cooling effect. The following diagram shows these 4 components.

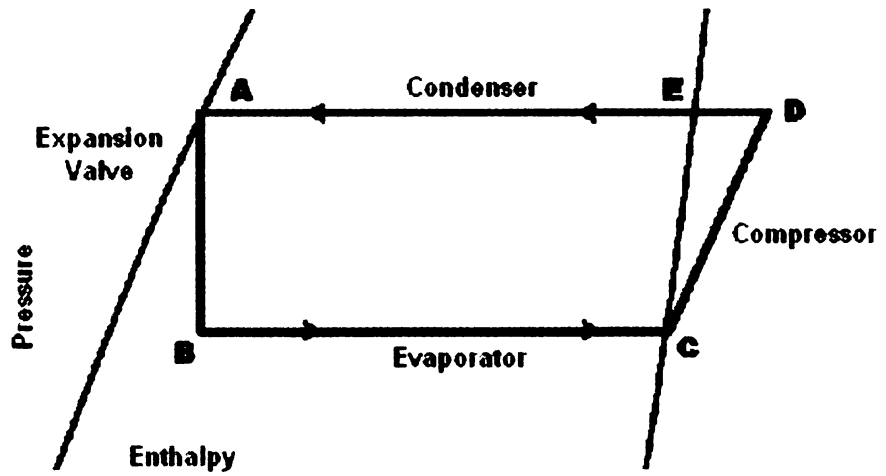

Figure 1. Ideal Refrigeration Cycle

The low evaporator pressure means that the mass flow rate through the compressor will be very small, and thus low power (around 250 Watts), is required to run the machine. The values for numerous refrigerants can be plotted and compared.

Table 1. Refrigerant Comparison Chart [9]

Ref	ODP	GWP	Ref. Cap. ($kj\,kg^{-1}$)	COP	π	Comp. out. temp. (°C)
R718	0[†]	0[†]	2309	5.70	10.0	223
R717	0[†]	0[†]	102.9	5.96	3.03	99
R12	1[‡]	8500[‡]	106.5	5.70	2.88	55
R22	0.034[‡]	1900[‡]	145.6	5.60	2.85	67
R290	0[‡]	20[‡]	250.1	5.42	2.66	54
R134a	0[‡]	1600[‡]	131.9	5.54	3.18	62
R152a	0[‡]	190[‡]	228.0	5.88	3.15	52

From this table, it is important to note a few characteristics. First, as stated earlier, the ODP and GWP of water is 0, which again means it has no harmful effects on the environment. COP represents the coefficient of performance, which in essence is how effective the refrigeration device is, the COP is simply calculated using

$$COP = \frac{CoolingEffect}{CompressorWork} \tag{1}$$

From figure 1, the COP is simply found by looking at the enthalpy change of the evaporator (the x – axis value) and the enthalpy change of the compressor. The chart shows that the COP of water is equal to or comparable to other common refrigerants. Also, the refrigeration capacity of water is much higher than its counterparts. Perhaps the most important data to pull from this table is the symbol π which represents the pressure ratio needed. Water requires a relatively high pressure ratio by the compressor and this is the most important challenge to overcome. This is why special care is taken in designing a drive system that can run a compressor to obtain such high ratios. Currently, there are a few commercial units being used worldwide that use water as the coolant and one can be seen below.

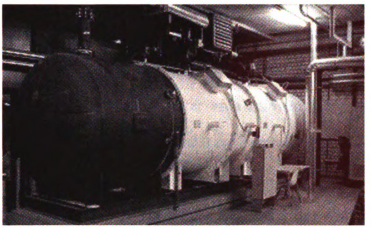

Figure 2. Water Chiller Examples

The primary drawback to these units, however, is their very large size. The high pressure ratios are only obtained using large radial compressors with diameters in the region of 1 meter. [9] The schematic of the above design can be seen below. In the diagram, the 2 blades represent 2 radial compressors, and the evaporator (what generates the cooling effect) is seen on the right.

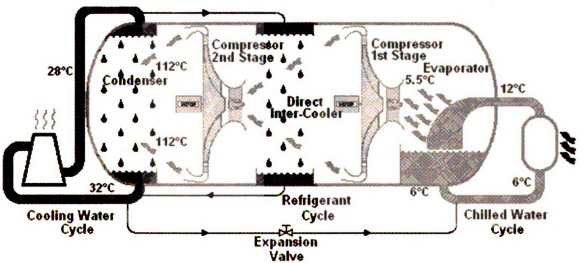

Figure 3. Schematic of Current Chiller Design

This large size means this device only has commercial and large scale applications. With most homes using AC during the summer months, this represents a huge untapped market. It would be advantageous to take these large devices and try to scale them down. This would allow water as a refrigerant to go from primarily commercial and large scale uses to a device that can comfortably sit in someone's home or backyard.

Two routes are generally proposed to create a small, home device. The first route, which is the topic of this paper, is to use a series of axial compressors to achieve such high pressure ratios. The second route uses a condensing wave rotor to aide in the compression. A schematic of the former case with the axial compressor stages can be seen below.

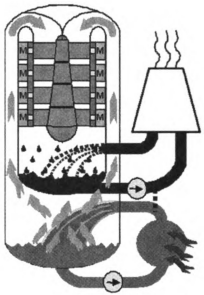

Figure 4. Schematic of Proposed Chiller Design

The primary feature of this design is the series of four axial, compressor stages arranged in series. These blades will be spinning at extremely high speeds, and this

thesis aims to devise a drive system to rotate these blades at high velocity. This can be accomplished in a novel approach that integrates the impellers into an electric motor, using the fact that the compressor blades are all composite and easily wound on a machine.

The alternative approach to using axial, compressor stages is implementing a wave rotor in the design. This has the benefit of helping to compress the fluid more, without the need of having numerous axial fans arranged in a series. The biggest drawbacks with a wave rotor are the precise complexities needed to setup such a device.

In the next section, we will briefly discuss the background behind the composite wound impellers used in the compressor.

Composite Impellers:

Water has many challenges regarding its use in a compact design. These include high, compressor, outlet temperatures. The solution is the design of a high-speed, multistage, counter-rotating, axial compressor. As opposed to very large rotors, (the large size means the tip speed will be very high at low RPMs), this design uses a small radius, spinning at extremely high speeds. An analogy that helps explain this is Euler's Equation.

$$\tilde{e} = u_2 c_{u2} - u_1 c_{u1} \tag{2}$$

In the equation above, u_2 is the tangential velocity at the impeller tip (outlet), $\tilde{e}$ is the shaft work, and c_{u2} is the tangential component of the fluid flow velocity. As the radius of the impeller increases, the tip speed increases, which increases the shaft work.

Because of these high rotational speeds, (on the magnitude of thousands of rpm), the impeller itself must be of extremely high quality, so that the forces imposed on the impeller don't cause it to tear itself apart. A composite impeller solves this by being both strong and lightweight.

The considered impeller can be generated on a commercial winding machine and have a radius of around 6cm. It can be made of several continuous fibers that are wet with polymer matrix material during the winding process and harden together to form a single piece. The winding machine is a simple device that takes carbon strands and winds them around objects, much like thread winding on a spindle. By precisely

calibrating and programming this machine, it can be made to perform a winding pattern that creates an impeller.

An example of this winding machine can be seen below. These machines are commercially available through numerous companies.

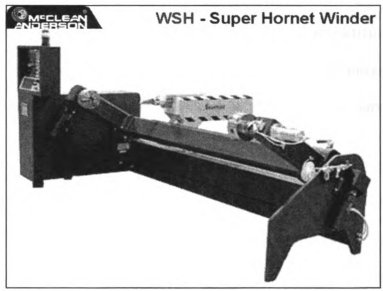

Figure 5. Composite Winding Machine

The biggest advantage of this winding machine is that it can make prototypes rapidly and quickly. As opposed to prototyping in a machine shop, modifications to the design can be made fast. An example of a woven impeller can be seen in fig. 6.

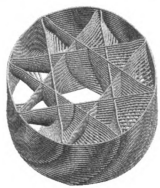

Figure 6. Example of a Composite Woven Impeller

Another aspect of this design is the resin bath in which the carbon fibers are dipped. After the impeller is wound, the resin can be left to set and harden. It is proposed that perhaps various materials, (such as powdered magnets), could be mixed in with the resin bath. This means that when the composite sets and hardens, magnetic materials will already be integrated in the design. By merely magnetizing this layer, the entire impeller could become a weak magnet. Also, instead of integrating magnetic material in the resin, magnets could be wound in with the fibers during the winding process.

Brushless Permanent Magnet Motors:

Brushless permanent magnet electric motors function on the basic principles that a current flowing through wound wires in a stator will generate an induced magnetic field that interacts with permanent magnets attached to a rotor. The stator is the part of the motor that houses and surrounds the rotor and also uses the windings to create the electromagnetic field. The rotor is the part of the motor that rotates and generally has permanent magnets mounted on its surface. The rotor is most commonly a shaft of some sort, used to drive some device. The most important component of the motor, therefore, is the torque that it generates at a certain rotational speed. Generally, for motor design, high torque is the ideal output. For our purposes, however, it is known that the impeller blades require very low power (250 W).

The motor design considered here is a direct current (DC) brushless permanent magnet motor. DC in this case means that the motor will have a trapezoidal back electromotive force (instead of a sinusoidal current in a pure alternating current AC motor). An example of the back electromotive force used in our application can be seen below

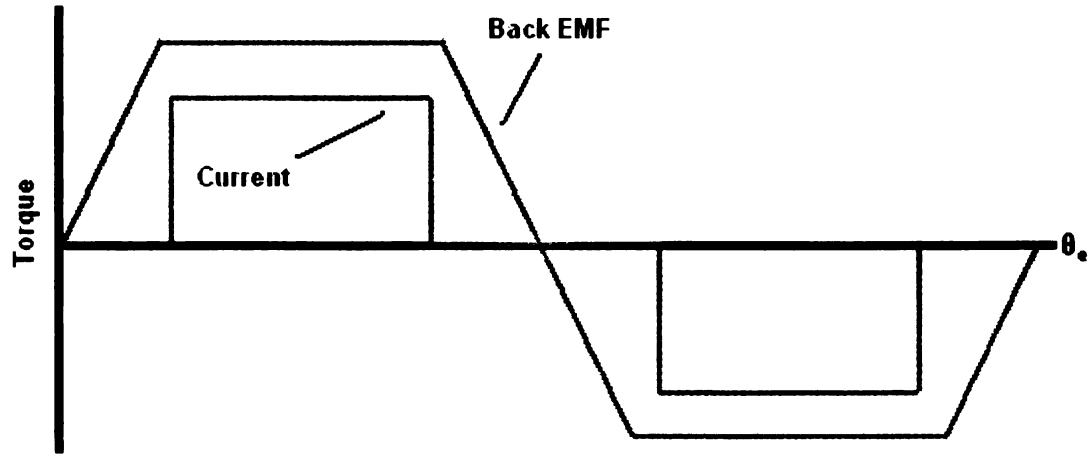

Figure 7. Trapezoidal Back EMF

At its simplest, a motor can consist of a single 2-pole (north and south) magnet as a rotor, surrounded by 2 stator slots with windings. Each pair of windings makes up a motor phase. When current is applied to the windings, a magnetic field is created through the windings and thus interacts with the magnet poles at the rotor in the center. By reversing the current, the polarization of the windings reverses.

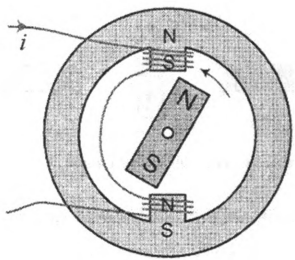

Figure 8. Simple 1 Phase 1 Magnet Pair Motor [4]

In the above diagram, the 2 magnet poles in the middle represent the "rotor", and the circular outer shroud represents the stationary "stator". Using this simple diagram, we can generate a basic torque characteristic of the motor. Intuitively, since the rotor magnets are closest to the magnetic field of the windings, they will receive the lowest force because the force is effectively locking the magnet in place. Conversely, as the magnets move further away from the stator teeth, the torque acting on the rotor will

increase. This torque characteristic follows a sinusoidal relationship and can be seen below.

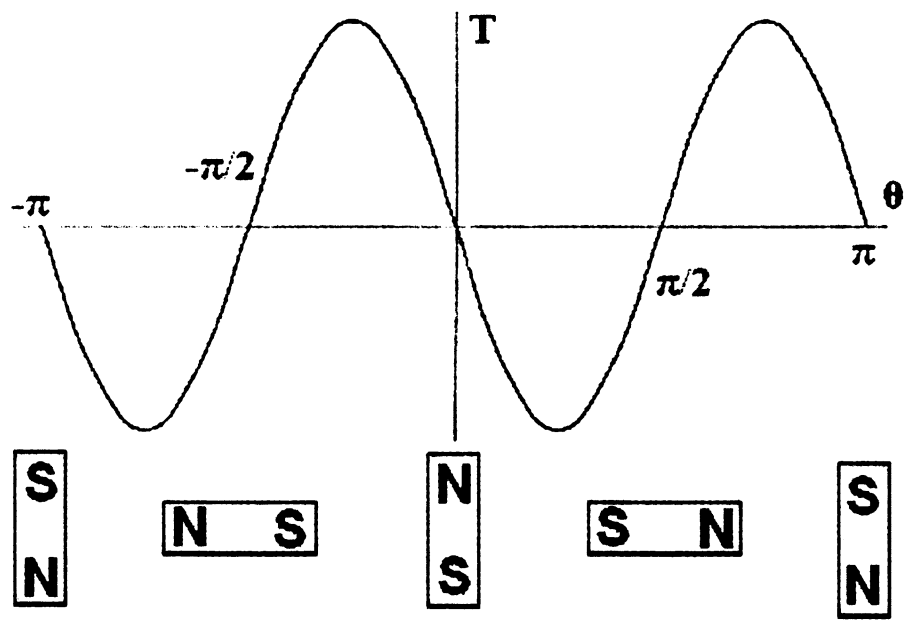

Figure 9. Sinusoidal Torque Characteristic [4]

Although the preceding example shows only 2 magnet poles and one phase, any combination of phases and magnet poles can be created so long as the number of rotor magnet poles is an even number and the number of stator phases is greater or equal to 1. An example of a 2-magnet pole, 3-phase motor can be seen below.

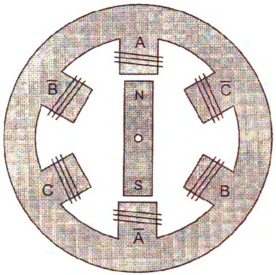

Figure 10. Example of 2-Magnet, 3-Phase Motor [4]

As the number of phases and poles increases, the torque characteristic on the rotor changes as well. An important distinction to make is the mechanical position of the rotor, and the electrical position. The mechanical position θ_m of a rotor is defined by the number of poles facing the airgap N_m, and the electrical position θ_e

$$\theta_e = \frac{N_m}{2} * \theta_m \tag{3}$$

So, if a motor with a 4-magnet pole (2-magnet pairs) rotor does one entire electrical rotation, it has only done 180 degrees of mechanical rotation. The electrical frequency f_e mechanical frequency f_m are related to each other through the number of poles.

$$f_e = N_p f_m \tag{4}$$

Thus, for a certain mechanical rotational speed, the electrical frequency required increases with the number of magnet poles. This is where the motor design is often constrained by the limitations of the input device (frequency converter) that is used to drive the motor. Therefore, fewer magnet poles are used for the design of high-speed motors to keep the electrical frequency down. The drawback for using fewer magnet poles, however, is that the torque production is much lower. The choice of number of magnet poles also ties into the efficiency and overall losses of the design.

For an efficient design of such a brushless motor, it is desirable to minimize the losses. Numerous losses and numerous variables are present. A motor constant has been derived to aid in the optimization of a motor. [4]

$$K_m = B_g R_m \sqrt{K_{wb} L_{st} N_m A_s / \rho} \tag{5}$$

With this equation, the objective is to maximize the value of the motor constant K_m, where B_g represents the airgap flux density, R_{ro} the rotor outside radius, K_{wb} the bare wire slot fill factor, L_{st} the length of the stator, N_m the number of magnet poles, A_s the area of the stator, and ρ the resistivity of the wires. The slot, fill factor is a measure of how well the wires fill the slots they are wound in. Because typical wires are round, it is impossible to have a slot with 100% of the volume filled by wires.

One of the most important parts of this equation is the air-gap flux density. This represents the magnetic field that is present in the region between the stator and the rotor. A high, flux density means a stronger magnetic field is present. This air-gap, flux density

is what is essentially driving the rotor and this is critical in the design of a motor. The flux can be found by

$$B_g = \frac{K_l C_\Phi}{1 + K_r \frac{\mu_R}{P_c}} B_r \tag{6}$$

where K_l is the leakage factor, C_Φ is the flux concentration factor, P_c is the permeance coefficient and μ_r is the relative permeability. [4] The remanence B_r, is based on the magnetic material chosen. The remanence can be found from tables regarding data on various magnets, which are readily available in online resources. The flux concentration factor is calculated by

$$C_\Phi = A_m / A_g \tag{7}$$

where A_m is the magnet surface area and A_g is the surface area of the gap. In equation (4), the leakage factor K_l is generally less than 1 and is difficult to obtain analytically; however, it can be determined quite easily and accurately using the finite element method. It is usually around .9 to 1.0. [3] The reluctance factor K_r represents the resistance that the non magnetic materials have, analogous to electrical resistance in an electric circuit. This value is generally in the range of 1.0 to 1.2. Much like the leakage factor, the reluctance is difficult to determine. The value μ_r represents the relative recoil permeability of the material, which is the permeability of the material, relative to free space ($4\pi \cdot 10^{-7}$ H/m). This value is typically between 1.0 and 1.2. These values represent quantities that are common for most electrical motors. Intuitively, the flux in the air-gap

B_g will be less than the residual induction of the magnet B_r. Also, the air-gap flux can't exceed this value, as this represents the upper bound on B_g.

The quantity P_c, is the permeance coefficient, and is found by

$$P_c = \frac{l_m}{gC_\Phi} \tag{8}$$

where g is the length of the gap and l_m is the magnet length. The permeance coefficient is determined based on the geometry of the surfaces. The value for the permeance coefficient is usually from 4 to 6 for magnet designs. This is due to the fact that this range aims to optimize the air-gap flux. Keeping all other values constant, the following graph shows how the permeance coefficient can affect the air-gap flux.

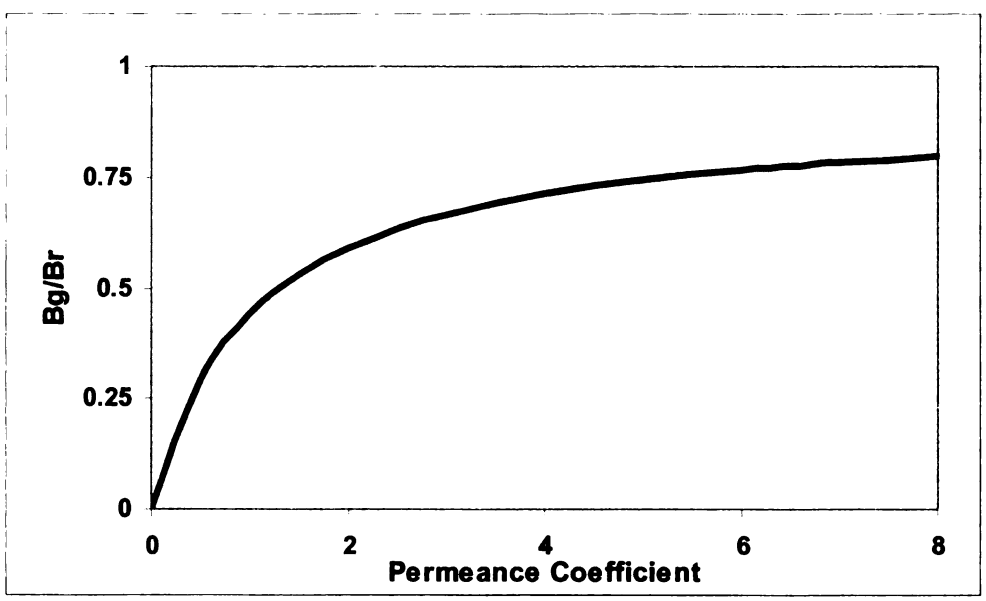

Figure 11. Permeance Coefficient Vs. B_g/B_r

At low values of permeance coefficient the magnet is very thin and thus the air-gap flux is small in comparison to the residual flux. As the magnet gets thicker and the permeance coefficient increases, the effective air-gap flux increase slowly becomes negligible. Thus, you are adding too much magnet to your design and obtaining not much net change on the air-gap flux. This value B_g/B_r can more simply be called the flux density. The larger the permeance coefficient the higher the flux density will be. For any motor a high flux density is desirable.

For simplicity, the air-gap can be modeled as a rectangular prism. [3] The diagram below shows the nomenclature used for calculating the permeance coefficient.

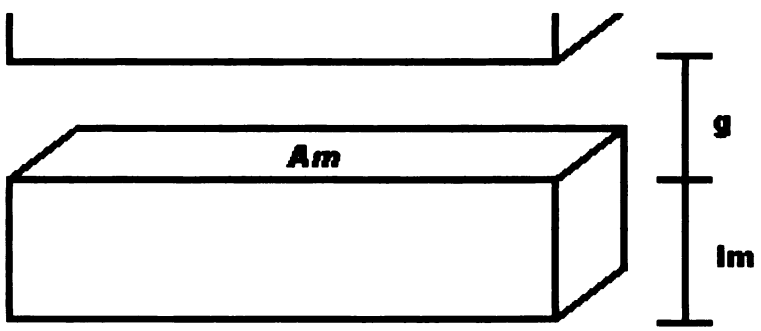

Figure 12. Permeance Coefficient Diagram

The flux concentration factor C_Φ is calculated by dividing the area of the magnet facing the gap and the area of the air-gap. For cases where the magnet is directly touching the air-gap, the flux concentration factor is simply 1. However, it takes on a different value if a retaining sleeve is between the magnet face and the air-gap.

These preceding equations and values can be used to get a simple value of the magnetic flux in the airgap. With the airgap flux calculated, the back emf for the motor e_b can be determined using equation 9 and equation 10.

$$e_b = 2N_m N B_g L_{st} R_{ro} \omega_m \tag{9}$$

The angular speed is ω_m, N is the number of wire turns, and R_{ro} is the radius to the outside of the rotor. For a sleeveless rotor, R_{ro} is the same as R_m. Lastly, an equation that relates the torque generated by the motor to the back emf can be shown as

$$|T| = \frac{|e_b| * i}{\omega_m} \tag{10}$$

where i is the current flowing through the wound wires.

The torque generated by the motor can be related to power by

$$T_{\max} = \frac{P_{\max}}{\omega_m} \tag{11}$$

This gives the maximum torque possible (no losses) with a given input power. The air-gap flux can also be used to determine the width of the stator teeth. The primary concern is ensuring that the flux flowing into the tooth is below the saturation level of the ferromagnetic material. [4] Exceeding the saturation level of the ferromagnetic material means the material is permanently altered and will have a degradation in magnetization. The flux on one stator tooth Φ_t can be calculated from total flux that is acting over all the stator teeth Φ_{total}

$$\phi_t = \frac{\phi_{total}}{N_s} = \frac{B_g 2\pi R_{ro} L_{st}}{N_s} \tag{12}$$

where N_s represents the number of stator teeth. This can be related to finding the teeth width

$$w_{tb} = \frac{2\pi R_{ro} B_g}{N_s K_{st} B_t} \tag{13}$$

where K_{st} is the lamination stacking factor. [4]

Lamination stacking is very important. The stator of a motor is not a solid piece of metal but rather thin sheets of metal which are pressed together. Between these sheets thin layers of insulating material are used. This means there is a lot mechanical and electrical resistance in the axial direction of the stator. This helps force most of the flux in the stator towards the center of the motor and not axially through the stack.

K_{st} is the ratio of the area of the steel, to the total area of the tooth in perpendicular direction. This value is generally in the range of 0.8 ... 0.99. The width of the stator yoke can similarly be found using

$$w_{sy} = \frac{\pi R_{ro} B_g}{N_m K_{st} B_{sy}} \tag{14}$$

The following diagrams shall aid in further understanding the dimensional nomenclature.

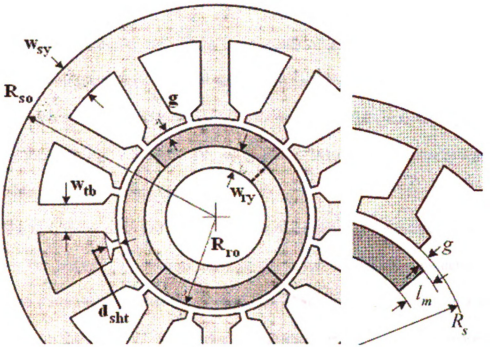

Figure 13. Nomenclature for Various Dimensions. [4]

It should be noted that the airgap flux neglects gaps due to slots in the stator. A diagram that models the magnetic flux through the various components of the motor can be seen in figure 14.

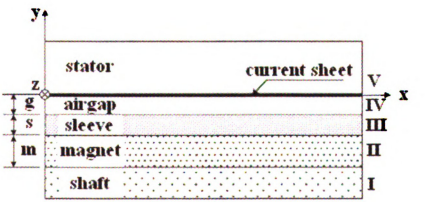

Figure 14. Simplified 1D model. [6]

This diagram shows the various components of a flux calculation and that all aspects of the motor can have an affect on the air-gap flux. This is the crucial coupling for the energy transmission from the stator to the rotor. For the calculations, we will be neglecting the shaft and will have a sleeveless motor. Also, a lot of internal resistances are accounted for in the various constants.

The next major aspect of motor design is determining the winding of the coils in the slots. The number of windings and how the motor is wound helps determine the shape of the stator teeth. Earlier it was mentioned that the number of slots in a motor is designated with the value N_s. This value is dependent on the number of phases in the motor. As a general rule of thumb, the number of slots in a motor must be a multiple of the number of phases in the motor.

$$N_s = \frac{N_m}{2} * k \tag{15}$$

The preceding equation relates the number phases $N_m/2$, to the number of slots N_s, using an integer called k. There are two types of winding methods that can be used, concentrated winding or distributed winding.

Concentrated winding is similar to the winding in figure 10. The windings of each phase are isolated from one another. More common, however, is the method of distributed windings. [4] In this method, instead of a winding going around only one tooth, windings span across multiple teeth. This grouping of multiple teeth under one

winding produces a pole for that coil. The following diagram illustrates this much more clearly.

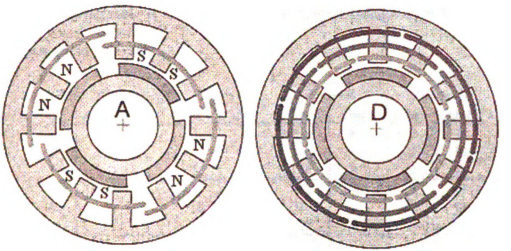

Figure 15. Distributed Winding [4]

In this diagram, it is clear to see that part A represents a single phase of the motor. This can be applied to any motor, with a different number of phases and magnet poles.

This introduces a new term called the coil span. The coil span outlines over how many stator teeth the coil will cover. The coil span can be found by relating the number of stator teeth N_s and the number of magnet poles N_m.

$$N_{sm} = \frac{N_s}{N_m} \tag{16}$$

In the preceding equation, N_{sm}, is the nominal coil span. For a 3-phase motor, each of the back emf must be 120° out of phase for each other. To simplify winding further, various literature and software is available that has common winding diagrams

available. This eliminates the need of figure out the winding diagram for your particular case. In the appendix, an example of a winding diagram is given.

The following table is an excerpt from the appendix diagram, and simply shows how the coils are to be wound.

Coil	Coil	Phase A		Phase B		Phase C	
No.	Angle, °E	In	Out	In	Out	In	Out
1	0	1	4	5	8	3	6
2	0	1	16	5	2	3	18
3	0	7	4	11	8	9	6
4	0	7	10	11	14	9	12
5	0	13	10	17	14	15	12
6	0	13	16	17	2	15	18

Figure 16. Winding Diagram [4]

This table is for a 6-magnet pole, 18-slot motor. All of the slots are numbered from 1 to 18 and correspond to the values in the table.

Another consideration regarding winding involves how the winding goes around each tooth in the stator. The coils wound can either be closer to the stator yoke (the outmost part of the motor, termed the "slot bottom") or closer to the rotor, the "slot top". Each slot must house two sets of windings, with one being in the slot bottom and the slot top. This difference is small enough to be negligible.

With a basic understanding of windings we can move on to calculate more dimensional characteristics of the motor. These are related to the stator teeth dimensions and the size of the stator slots.

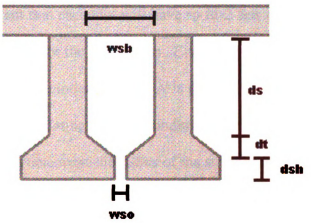

Figure 17. Stator Slot and Teeth Nomenclature

The first thing we can calculate is the width of the slot opening w_{so}. This opening exists so that the wires used in the windings can be easily wound around the teeth. Thus, the value is merely dependent on the size of the wires used. The slot opening should be 2 to 3 times the size of the covered wire diameter.[4] For a nice size, we can simply say that

$$w_{so} = 2 * D_{wire} \tag{17}$$

where D_{wire} is the diameter of the wire gauge chosen. The value for d_{sh} is similarly arbitrarily chosen. This is the shoe tip depth. For simplicity the shoe tip depth will be the same as the slot opening. Next we need the shoe taper depth d_t. Similarly, this can be chosen to be ½ the size of the shoe tip depth d_{sh}.

With these dimensions chosen, we can start working towards finding the windable slot depth d_s. As the name implies, this length indicates the amount of room there will be for the windings to fit in. Earlier in figure 15, we looked into distributed winding. Using

this figure it is apparent that each slot will have to fit 2 sets of windings. These can be wound either in the slot top or the slot bottom. Either way, this implies that each slot will have to accommodate $2*N$ windings, where N is the number of windings required. This fact will be used when calculating how the windings will fit in each slot.

First, we need to determine the radius of the stator at the beginning of d_s, which is the location where the windings will begin. Using the diagram regarding the tooth dimensions and figure 13, we can find this value by using,

$$d_{s1} = R_m + g + d_{sh} + d_t \tag{18}$$

where d_{s1}, signifies the start of the windable slot depth. Next, to simplify our winding method, we will assume that the slot area will be a perfect square instead of an arc. Given the fact that there will be a relatively small difference in the arc lengths in our design, this is reasonable. The following diagram shows the new nomenclature.

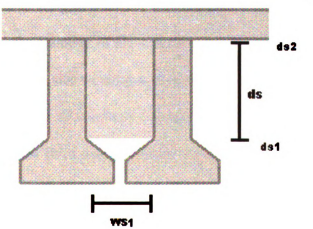

Figure 18. Slot Nomenclature

With d_{s1} solved for, we can calculate the value for the slot width w_{s1}. This is found by using

$$w_{s1} = \frac{2\pi(R_m + g + d_{sh} + d_t) - N_s * w_t}{N_s} \tag{19}$$

This equation solves for the circumference of the stator at the point d_{s1}, then subtracts the total thickness of all the stator teeth and finally divides it by the number of slots. Now we can begin to determine how the windings will fit in the slot.

In order to wind this, we will say that the windings for the left tooth in figure 18 will cover both the slot top and bottom, but will remain in the left half of the slot opening. Thus, the slot width we will be working with, will be ½ the value for w_{s1}. After this initial slot winding is finished there should be ample room to rewind each slot such that the slot bottoms and tops are wound.

A simple understanding of standard wire gauges is required and will be explained a little later. For now, the diameter of the wires is going to be merely described as D_{wire}.

We can start out the slot winding analysis with the value N, which in equation 9 represented the total number of windings that are needed for each stator tooth. We also know these windings must fit in a slot of width $w_{s1}/2$, with a height of d_s. Also, we can only have integer values of N because it is impossible to do fractional windings. Thus, the value for N will be rounded up. We also will associate a wire gauge diameter called D_{wire}, with this winding number.

First, lets determine how many windings we can fit going across in a straight line of length $w_{s1}/2$. This is simply done using

$$N_{across} = \frac{w_{s1}}{2 * D_{wire}} \tag{20}$$

which gives us the number of wires that can fit across in the length $w_{s1}/2$. It is important to note, that if the value for N_{across} is a decimal, it means that the last wire will only be a fractional part of a wire. Therefore, we must round down this value of N_{across}. Now we have a value that shows us how many wires can fit in a row of our slot. With this determined, we can work up, and figure out how many vertical rows of wires we need. This is done using a similar equation.

$$N_{up} = \frac{N}{N_{across}} \tag{21}$$

Similarly to before, this value can come out to be a decimal, which means we need a fractional number of vertical rows. In order to ensure we have the correct number of windings N in our device, we round this value up. The final result is a number that gives us the number of winding rows and columns we need in order to fit the windings in half of a slot. The diagram below shows the previous equations explained in more detail.

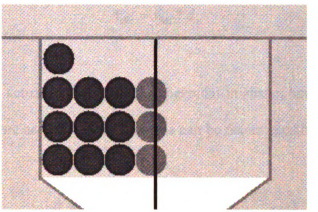

Figure 19. Winding Diagram

In this picture the circles that are over the black line represent wires that would be the fractional amount. Thus, in a row, the number of wires is rounded down from 3.75 wires to 3. Similarly, in the vertical value needed to be rounded as well, to accommodate the 1 wire that is leftover. Once this is completed however, this winding method can be shifted to wire each phase in either the top half of the slot or the bottom half. (This example wound it in the left of the slot, and the right of the slot) This is consistent with the method mentioned earlier.

With the winding completed, the end goal of determining d_s can finally be completed using the following equation,

$$d_s = N_{up} * D_{wire} \tag{22}$$

which simply multiplies the number of rows needed, by the diameter of the wire.

For this case, we simply modeled the area of the slot as a square that is found by using:

$$A_{slot} = w_{s1} * d_s \tag{23}$$

However, the actual slot is roughly trapezoidal in shape, bounded on the top and bottom by 2 arcs. More accurately, the slot area can be determined by [4]

$$A_{slot} = \frac{\pi}{N_s}\left[\left(R_{so} - w_{sy}\right)^2 - \left(R_m + g + d_{sh} + d_t\right)^2\right] - w_{tb} * \left(R_{so} - w_{sy} - R_{ro} - g - d_{sh} - d_t\right) \tag{24}$$

This value of the slot area can be used to determine the slot fill factor. The slot fill factor shows how densely packed the wires are in the slot and how much of the slot consists of wire instead of empty space. The slot fill factor is found by

$$K_{wb} = \frac{2N * .25 * \pi D_{wire}^{\ 2}}{A_{slot}} \tag{25}$$

Due to the fact that wires are round and not square, a fill factor of 1.0 is impossible to obtain. Also, layering the wires like we did in figure 19 is the least efficient way to pack in the wires. The most efficient way would look something like in the figure below.

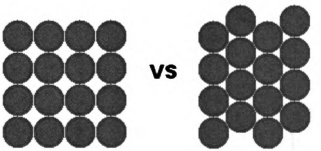

Figure 20. Efficient Wire Packing Method

By doing this type of packing, the slot fill factor increases by a few percent. For the sake of simplicity in calculation, the row/column model in figure 19 will be used. This is a more conservative approach. Also, we are not taking into account whether the wire is covered with insulation or bare. However, in [4], it was mentioned that with reasonable costs it is possible to obtain a value of K_{wb} in the range of 50% fairly easily.

Another key aspect of motor design is the slot correction factor. Earlier in equation 6 we determined the flux across the air-gap. This calculation assumed a constant air-gap in the motor. However, we know that this is not true. Periodically, a rotor point will pass by a slot opening (with length w_{so}), which means the effective air-gap at this point increases, thus changing the air-gap flux calculation. When passing this slot opening the airgap now becomes the length from the rotor to the inside of the stator. This is shown in the following diagram.

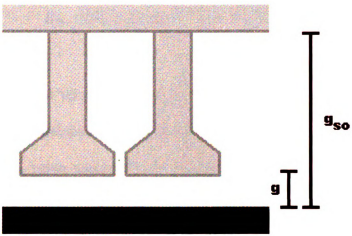

Figure 21. Slot correction factor diagram

This new opening width is denoted as g_{so} and represents this new air-gap length which occurs as the rotor passes the slot opening. Or, we can say that θ_s represents the angle for the tooth head and slot opening and θ_t represents the angle of the tooth head. The difference of these two angle measures is the angle of the opening of the slot. We can then say that the air-gap g, is a function of the angle, $g(\theta)$. This can be integrated into equation 6 to give us an equation for the slot correction factor[4].

$$K_{sl}(\theta) = \frac{1 + \frac{P_c}{K_r \mu_R}}{\frac{g(\theta)}{g} + \frac{P_c}{K_r \mu_R}} \tag{26}$$

The value of $g(\theta)$ ranges from the normal air-gap value of g, (in which case that fraction becomes 1), to a max value of g_{slot}. The value of g_{slot} is simply calculated by one of the following 2 equations.

$$g_{slot} = \left(R_{so} - w_{sy}\right) - R_m = g + d_{sh} + d_t + d_s \tag{27}$$

This function can be plotted on a graph of K_{sl} versus θ, where θ is the current location over the tooth and slot opening you are at.

With this g_{slot} value, there will also be a permeance coefficient associated with it. Much like in figure 12, we can use equation 8 to find the permeance coefficient for this air-gap. This is given by a slightly modified equation.

$$P_c = \frac{l_m}{g_{slot} C_\Phi} \tag{28}$$

Because of the increased air-gap this permeance coefficient will be much smaller than its counterpart.

With equations for all of the dimensions determined, we can easily calculate an estimate for the total mass of the magnets, stator and wire windings. This is done considering the fact that the stator and rotor are essentially hollowed out cylinders. The densities of the magnets, stator material and wire are all known, thus a simple volume calculation will lead to the masses.

To find the volume of the stator, the key values are the stator inner radius R_{si}, stator outer radius R_{so}, and the teeth dimensions d_s, d_t, d_{sh}, w_{so}. With the slot area determined in equation 24, this further increases the simplicity of the calculations.

First we can calculate the volume of the stator, starting from the windable slot depth d_1, going out to the outer stator. This is done using

$$V_{stator1} = \left[\pi\left(R_{so}{}^2 - d_{s1}{}^2\right) - N_s * A_{slot}\right] * l_{st} \tag{29}$$

where l_{st}, signifies the length of the stator. Next, we need to add in the volume of the teeth that lay below the windable slot area. To simplify this, we can model these as squares and triangles, like below.

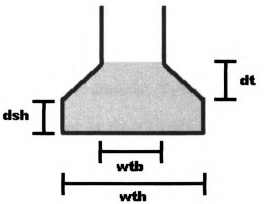

Figure 22. Tooth Head Diagram

Finding the volume of the tooth using this diagram is done using:

$$V_{stator2} = \left(w_{th} d_{sh} + 1/2 * (w_{th} - w_{tb}) * d_t + w_{tb} * d_t\right) * N_s * l_{st} \tag{30}$$

Using both of these equations, we can get the total volume of the stator by adding them together. Finally, using the density of the stator material ρ_s, we can obtain the mass.

$$M_{stator} = (V_{stator1} + V_{stator2}) * \rho_{stator} \tag{31}$$

Next, the mass of the magnets can be obtained. Because the magnets are a thin ring around the rotor this is a very easy calculation and is the same calculation for a hollowed out cylinder. The density of the material is signified by ρ_m.

$$M_{magnets} = \left[\pi * (R_m^{\ 2} - R_r^{\ 2}) * l_{st}\right] * \rho_{magnet} \tag{32}$$

Lastly, the mass of the wire can be calculated. This is done by estimating the wire length, and assuming a constant wire diameter. To estimate the length of the wire we can use a few facts. First, the wire can be modeled as being wound in a square around the stator teeth. Because we would be using distributed winding, this means the windings will span a few teeth. Thus, we can model it like below.

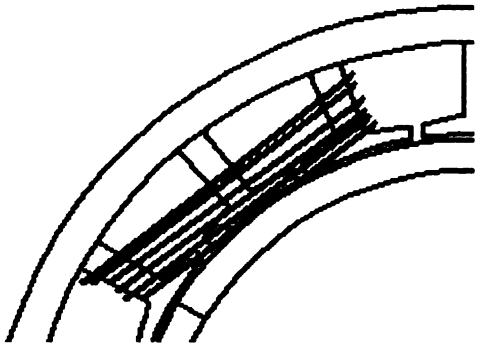

Figure 23. Winding Length Diagram

Used in conjunction with figure 17, we can obtain a simple expression to calculate the total length of wire in 1 winding as follows

$$L_{winding} = 2\left(l_{st} + 2w_{s1} + 3w_{tb}\right) \tag{33}$$

Using this equation, finding the total length of all the wires in the stator is found by using,

$$L_{wires} = 3L_{winding} * N * N_m \tag{34}$$

where the 3 represents the 3 phases of the motor. To find the length for 1 phase, we would simply divide the preceding equation by 3. Finally, this equation can be used to find the total mass of the wire.

$$M_{wire} = L_{wires} * 1/4 * \pi D_{wire}^{2} * \rho_{wire} \tag{35}$$

where M_{wire} signifies the total mass of all the wires and windings in the motor. This merely represents a rough estimate. Finally, we can integrate all these mass equations together to get an initial estimate as to the total weight of the motor.

$$M_{total} = M_{wires} + M_{stator} + M_{magnets} \tag{36}$$

This value can be used to help optimize our design by trying to minimize the overall mass of the device.

Finally, we can integrate all the preceding equations to obtain a simple efficiency calculation. Any motor designed will not operate at 100% efficiency. Losses due to heat, resistances in the wire, eddy currents and cogging torque will aim to reduce the

effectiveness of the motor. At extremely high speeds these effects become more and more prominent and need to be addressed.

One source of loss in a motor is common electrical losses in the wiring. Any conducting material is not perfect and has an internal resistance in it. Given the fact that our wires are not superconductors, there will be losses present. These power losses (in the form of heat), can be determined using the simple equation below

$$P_{slot} = I^2 * R_{slot} \tag{37}$$

where R_{slot} is the resistance of the slot. This resistance is calculated by[4]

$$R_{slot} = \frac{\rho l_{st} N^2}{K_{wb} A_s} \tag{38}$$

Combining these two equations together gives us a simple expression for the losses from wire resistances in the slot. It should be noted that these losses are fairly small in magnitude compared to other loss calculations.

Next, we can calculate the eddy current losses in the motor. Simply put, eddy currents are circulating flows of electrons generated inside of the conductor. This circulating flow creates its own magnetic field that opposes the magnetic field being generated in the stator.

In [10], the eddy current losses were shown to be calculated by

$$P_e = \frac{\pi B_g^{\,2} \omega_e^{\,2} (D_{wire}/2)^4 (L_{wires}/3)}{8\rho} \tag{39}$$

All of the loss equations can be added together to obtain the total power losses in the motor. The efficiency can be determined by

$$Efficiency = \frac{P_{stage} - P_{losses}}{P_{stage}} * 100 \tag{40}$$

This, in conjunction with the total weight, gives us two important parameters towards obtaining a lightweight and efficient motor design. Other losses can be more accurately determined by using the finite element method to model the motor.

Magnetics:

The design of a motor hinges on the proper selection of a magnetic material to be used in the rotor. For the particular design introduced here, the permanent magnets will be modeled as located on the surface of the impeller.

A permanent magnet is one that is capable of maintaining a magnetic field without excitation and magnetomotive force (mmf). In other words, this is an object that generates a magnetic field without the continual need of inputs. A permanent magnet is created by placing a metal alloy in a large mmf field. Upon removing the mmf field, a residual magnetic field value B_r will remain. If a subsequent mmf is applied to the magnet, the operating point of the magnet will move. [11] This can be plotted on a chart, and will form a hysteresis loop.

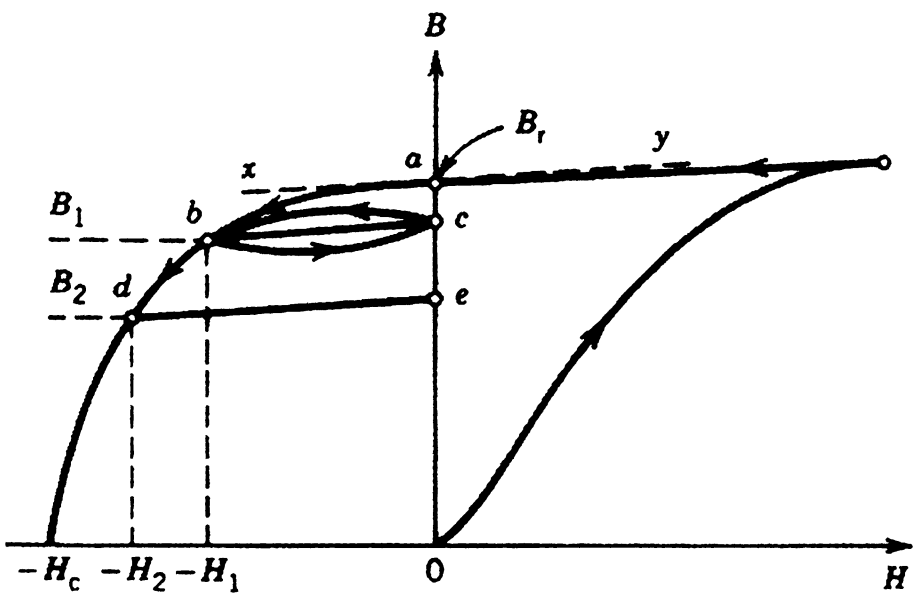

Figure 24. Hysteresis Loop [11]

A hysteresis loop shows how the magnetic field value B, relates to an input magnetic field intensity H. As long as the magnetic field intensity H does not exceed the initial magnetic field value B_r, the magnet is considered to be reasonably permanent. The hysteresis loop is important because it shows the operating points of the magnet.[3] The slope of the B-H curve at any single point is known as the relative differential permeability and is simply the ratio of magnetic flux density to magnetic field intensity. The diagram below is helpful in showing how the flux flows through a typical motor.

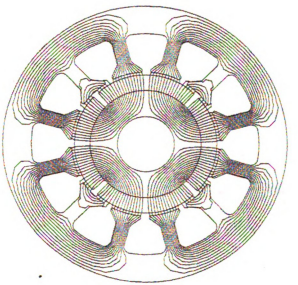

Figure 25. Flux Diagram [4]

In motor design, there are a few primary classes of magnets used. These include Alnicos, Ferrites/Ceramics and Rare earth metals.

Alnicos have the advantage of maintaining high magnetic flux over large air-gaps, but have tendencies to be demagnetized. Ferrites are generally the most popular due to their low cost and high electrical resistance. The last type of magnets are the rare-earth magnets. Although these are best choice for most applications, they have relatively

higher costs associated with them. Rare-earth magnets generally contain iron, nickel and cobalt combined with other rare earth elements.

Alnico's have the primary advantage of having low temperature coefficients. An alnico magnet has a temperature coefficient of around B_r, -.02%/°C and a maximum temperature of 520°C.[3] Alnico's generally have higher remanences than ferrite magnets, but are usually less than various rare earth magnets. These magnets derive their name from the fact they contain aluminum, nickel, and cobalt. Alnico's are also very brittle and should not be used as structural components in any device. Alnico's can be either cast, sintered or bonded.

Being cast is similar to any other casting process. This is where you pour molten metal into a mold. Sintered magnets are created by pressing small particles of the magnet in a press and then sintering them to create a solid magnet. Bonding is a die pressing process where magnetic particles are mixed with an epoxy binder which are then heat cured. Most magnets can be created using these 3 methods. Sintered magnets have a higher residual induction than bonded magnets due to the fact a bonded magnet contains the epoxy binder.

Ferrites have relatively high temperature coefficients. These are usually around B_r, -.2%/°C, with a maximum service temperature of around 400°C. Ferrites are extremely popular due to their low cost, however, they have comparatively lower residual inductions than their counterparts.

Rare earth magnets, are the most expensive magnets but have the highest residual inductions. They are generally made from Cobalt and Samarium (SmCo) or Neodymium, Iron and Boron (NdFeB). For a SmCo magnet, the temperature coefficient is around B_r,

-.03%/C up to -.45%/°C, with a maximum temperature of 300 to 350°C. An NdFeB magnet has a temperature coefficient of B_r, -.09%/C up to -.15%/°C, with a maximum service temperature of 250°C.[3] SmCo magnets thus have a higher temperature resistance but also a much higher cost associated with them.

Beside the proper arrangement of the stator windings, the design of a brushless permanent magnet motor needs to consider how the magnets on the rotor are arranged. The rotor magnets can be arranged in various ways.

First, the magnets can be arranged in array where all the magnets are charged radially as shown to the right in figure 26

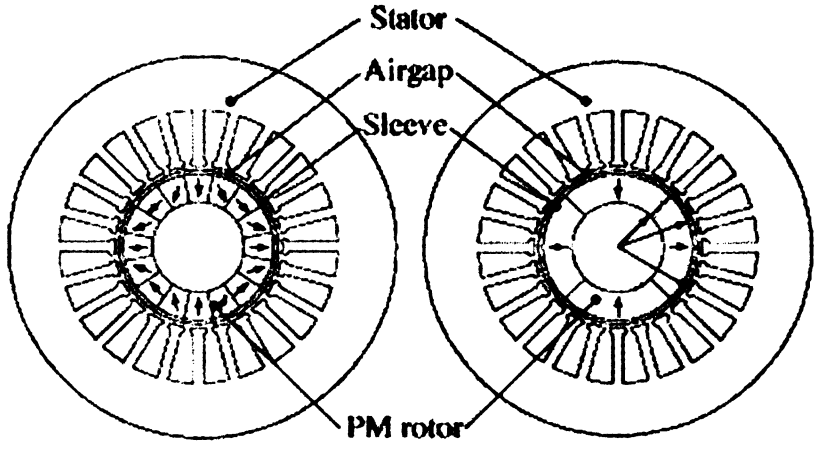

Figure 26. Halbach magnetized 4 magnet rotor (left), versus a parallel magnetized rotor (right).

This magnetic configuration is usually the simplest to implement and costs the least.

However, a Halbach array on the left in figure 26, arranges the magnets differently to produce a more ideal magnetic field.

In a Halbach array, the magnetic flux generated by the magnets is concentrated on one side of the array and is effectively cancelled out on the other.

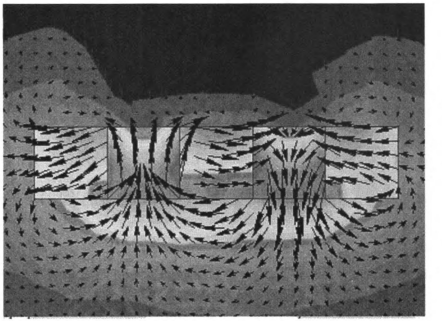

Figure 27. Magnetic flux from a Halbach array. [17]

Such an array has numerous advantages. First, they have a sinusoidal air-gap field distribution. This is different than a square wave field distribution obtained with discrete radial magnets. Also, an array of this nature has negligible cogging torque. Cogging torque is when motor permanent magnets try to align themselves with a maximum number of ferromagnetic materials.[16] This results the torque pulsations felt when the motor shaft is rotated by hand. [4]

As shown in figure 26, a brushless permanent magnet motor can utilize a Halbach array arranged in a circle to surround the rotor. In a simple Halbach array this sequence requires only two magnets for each pole. However, by utilizing more magnets in each sequence, the magnetic field generated by the Halbach array becomes more ideal.[16]

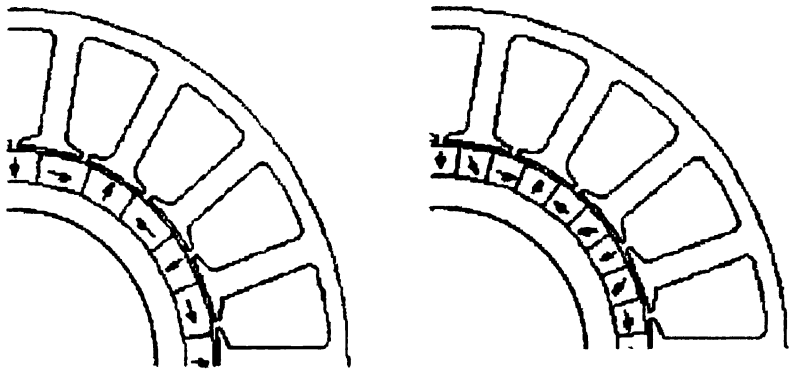

Figure 28. Two segments per pole Halbach machine (left), and three segments per pole (right)[16]

The airgap flux from an ideal Halbach array can be calculated as outlined in [12]. This equation is given below.

$$B_{airgap} = \frac{-2B_r \frac{p}{1+p}\left[1-\left(\frac{R_r}{R_m}\right)^{p+1}\right]\left[\left(\frac{r}{R_s}\right)^{p-1}\left(\frac{R_m}{R_s}\right)^{p+1}+\left(\frac{R_m}{r}\right)^{p+1}\right]\cos(p\theta)}{K\left(\frac{R_r}{R_m}\right)^{2p}\left[(1-\mu_r)+(1+\mu_r)\left(\frac{R_m}{R_s}\right)^{2p}\right]-\left[(1+\mu_r)+(1-\mu_r)\left(\frac{R_m}{R_s}\right)^{2p}\right]} \quad (41)$$

In this equation, p is the number of magnet pole pairs, (N_m/2), r represents the current radius you are at ($R_m<r<R_s$) and θ is represents what angle around the rotor you are currently at. Also, K is a value that is 1 for an iron cored rotor and $(1-\mu_r)(1+\mu_r)$ for an air cored rotor.

Frequency Drives:

To drive the electric motor an alternating current must be supplied to all three phases of the motor. The higher the rotational speed of the motor, the more expensive the frequency drive will have to switch the currents.

Earlier, the concept of electrical frequency was introduced. This is dependent upon the number of magnet pole pairs in the motor. The electrical frequency is the frequency at which the current must switch in order to have the motor rotate at its desired mechanical frequency.

In order to obtain the trapezoidal back emf in the motor, a square wave pulse of current is required. There are few types of circuits that can be used to supply current to a phase. These include a half bridge, a full h-bridge topology and a Y-connection.

A half bridge is much cheaper in cost, and only supplies current to one phase at a time. Thus, if phase 1 has current supplied to it, the 2nd and 3rd phases are not being used. The trade off of this however, is a much lower torque production[4]. This is present in low power applications where cost needs to be minimized and torque production efficiency isn't important.

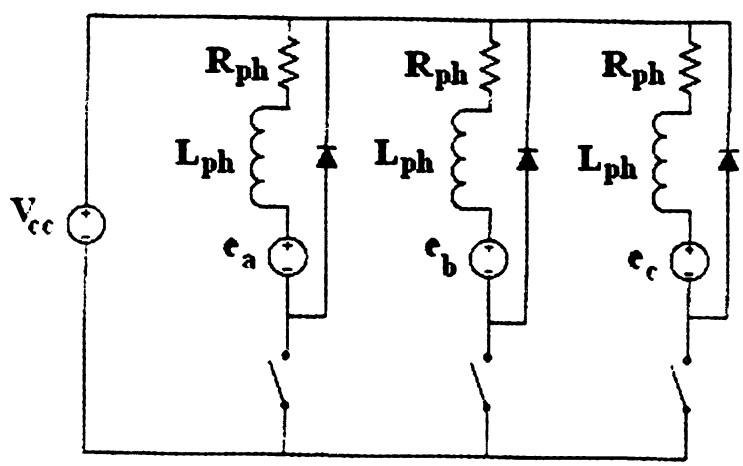

Figure 29. Half Bridge Drive

The full h-bridge topology is much more complex. It allows independent control of each phase current. [4] This is much more complex than the preceding example. This requires many more transistor switches and is more expensive. In the following diagram, this represents a full H-bridge that would control one phase.

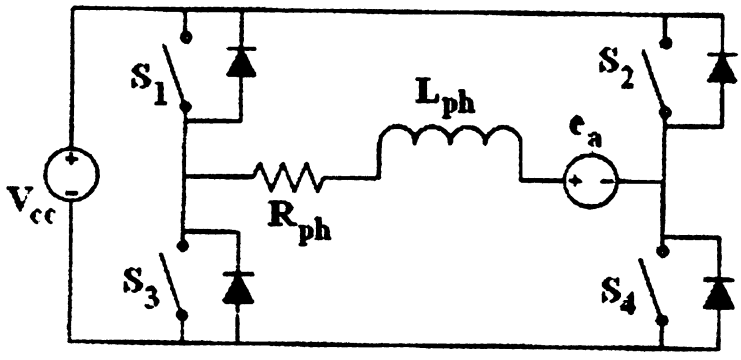

Figure 30. Full H-Bridge Drive

The most common type of topology used is a Y-connection configuration. However, the current of 2 of the phases is dependent on the current of the first phase. Thus, each phase cannot be controlled independently, like in a full h-bridge. But this topology allows for more torque production, since all phases are running and allows it a reasonable cost.

Magnetic Selection

Above, basics regarding magnets and magnet arrangements were discussed. The compressor in consideration shall operate at high efficiency, with a high rotational speed. Each magnet choice and arrangement should be heavily weighed and critiqued.

Ideally, with a composite impeller created on a winding machine, the best choice for a magnet would be one that could be integrated into the impeller itself. The best choice may be the addition of magnetic powder in the matrix material (resin) at the outer diameter of the impeller.

The first step is deciding which magnets should be used in the rotor. Various references on brushless magnet design generally favor the use of the rare earth magnet NdFeB[8, 9, 10]. Although rare earth magnets were generally associated with much higher costs, advances in the manufacturing of NdFeB magnets now have driven the cost down further. [3] The drawback from this magnet is that it is strongly temperature dependent. It is easily demagnetized at high temperatures and cooling the magnets is extremely important for the utilization of NdFeB.

For the application of being used to rotate an axial impeller in a small or medium size R718 chiller, the torque requirements are very low (typically <0.1 ... 1 Nm). Therefore for this purpose, NdFeB magnets generate an unnecessary strong magnetic field. Furthermore, NdFeB magnets are relatively more expensive than other magnet choices. Due to the fact that this impeller motor will eventually have commercial

applications, the utilization of these magnets may increase the price of the refrigeration or air conditioning unit.

Ferrite magnets seem to be the ideal choice for this application. First, ferrites are cheap to manufacture which helps keep the price of the motor unit down.

Another consideration is the temperature range of the magnets. Ferrites have a maximum service temperature up to 400°C. Also, ferrites are most economical in low horsepower motors due to their cheap price and low B_r. They also have low eddy current losses. [3]

For the overall design, various magnet types will be investigated. These can be seen in the table below

Table 2. Magnet Choices

Magnets	B_r	Density kg/m^3	Br/Density
Sin. Fe	0.35	4900	7.14E-05
Sin. NdFeB	1.2	7500	16E-05
Bonded NdFeB	0.5	7500	6.66E-05
Sin. Alnico	0.75	5700	13E-05
Bonded Alnico	0.35	5700	6.14E-05
Sin SmCo	0.9	7500	12E-05
Bonded SmCo	0.55	7500	7.333E-05
Magnet Paste	0.1	4900	2.04E-05

Next, the array type needs to be investigated. Two primary types of arrangements exist, a simple radial charging where each magnet pole is charged in only the radial direction, or a Halbach array where the two or more magnet segments make up a magnet. The Halbach array has the advantage of reducing the cogging torque. Also, a Halbach array is self shielding and requires less iron backing. [12] In [6], it was shown that for high speed permanent motor applications, a Halbach magnetized rotor has less rotor losses than a radially magnetized rotor.

Earlier, the calculations used assumed radial magnetization, which gave a perfect square wave magnetic field in the air-gap. Even though a Halbach array would be the best choice for this high speed motor, this simplifying calculation will still be used.

The next major criteria relating to the magnet arrangement is the number of magnets in a sequence per pole. As stated before, the more magnets used in a Halbach sequence, the more ideal the magnet is.

In [16], a method has been described, where instead of numerous magnets (each individually magnetized) being used to create the Halbach array, a high performance nearly ideal Halbach array can be created. This is accomplished by orienting anisotropic NdFeB powder during the injection molding process and magnetizing them with the required Halbach field.

However for a ferrite magnet, this may not be possible, thus the array may need to be created of numerous discrete magnets. A compromise needs to be found in terms of the number of magnets in the sequence per pole versus an ideal Halbach array.

Lastly, the total of magnet pole pairs should be chosen. For such a high speed application, the number of magnet pole pairs should be minimized. A lower magnet pole number, however, also necessitates thicker back iron on the stator and rotor in order to limit magnetic saturation. [14] A lower pole number also drives the cost down of the frequency generator that will be required to drive the motor. As the number of magnet pole pairs increases, the electrical frequency of the motor increases. (remember, the mechanical frequency will remain constant). For our design, we will only investigate low magnet pole pair numbers. So in our design spreadsheet, only 2 magnet pole pairs, and 3

magnet pole pairs will be considered. This should be sufficient to keep the electrical frequency low enough, such that the cost of a frequency drive will be lower.

Impeller Considerations

Some of the concerns regarding the integration of the motor into the impeller are whether or not the impeller itself can be magnetized or whether a ring of magnets needs to be affixed on it. Given that the lifespan of the motor is intended to be years, the magnets used for the motor should be resilient magnets that won't degrade noticeably in quality over such a long period of time.

Due to high centrifugal forces for rotors of relative large diameters, the magnets must use a retaining sleeve around them to attach them to the rotor. In many cases, the magnet is simply glued to the rotor. This is usually favored since magnets are brittle and not malleable. However, high rotational speeds mean that the glue may not be sufficiently strong. This retaining sleeve should be nonmagnetic and ideally would not contribute many losses. A sleeve with some conduction leads to eddy currents that cause rotor losses. [1]

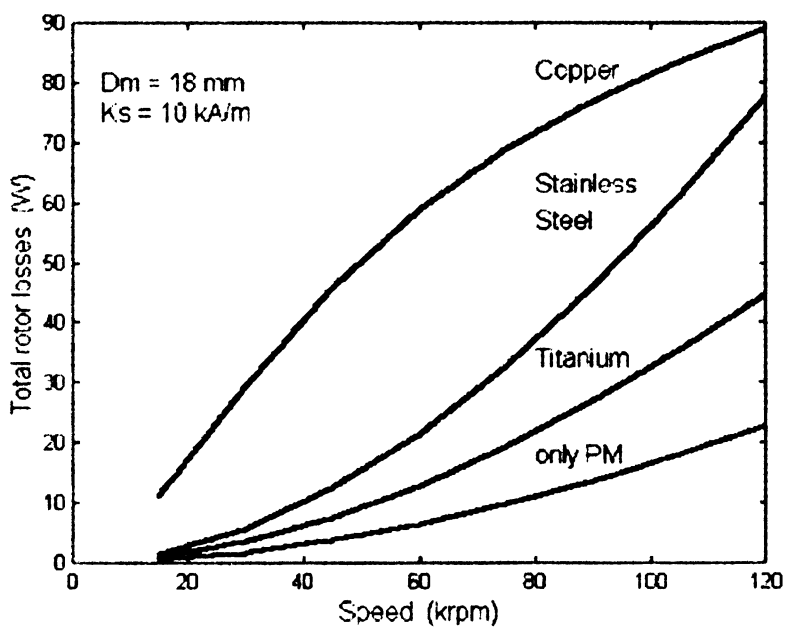

Figure 31. Total rotor losses for slotless stator for different retaining sleeve materials.[1]

Figure 31 shows losses as they depend on the material used in the retaining sleeve. This material selection is also related to costs and to how efficient the rest of the design is.

So far, we've only discussed using permanent magnets arrayed around the perimeter of the rotor but there is another innovative method that is being considered.

As stated earlier, the composite impeller is created using a winding machine. The carbon fibers, prior to being wound, are dipped in a solution of a liquid resin. After setting, the resin hardens which gives the impeller its strength.

Generally this resin solution is used as a binding and strengthening agent to keep the rotor together, however, various materials can be mixed in with the resin as well. It is theoretically possible to integrate magnets into the resin, so that when the impeller is wound it already has magnets throughout its design.

A magnetic powder can be used with the resin and subsequently magnetized. Currently, magnetic hardening resin has been applied to micro fabrication techniques.

In [5], a method was described that uses resin bonded magnets in Micro-electrical mechanical-systems applications (MEMS). The paper explains how difficult it is to produce magnets on a substrate. First, a powered Ba-ferrite or Sr-ferrite substance was used. This is due to the fact that the powder size of these magnets is sufficiently small (on the scale of 1 μm), as opposed to 10 μm for various rare earth magnets. The method of placing the magnet on a substrate can be seen below.

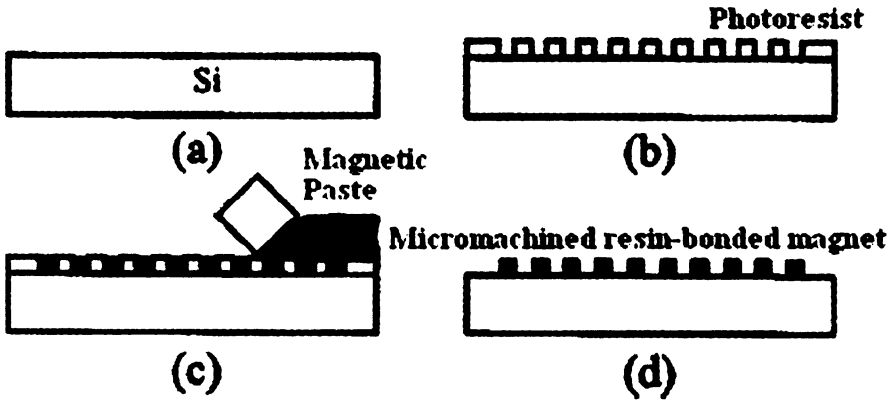

Figure 32. Micro magnet fabrication on a substrate.[5]

First, (a) shows the substrate (in this case a silicon wafer), with nothing on it. Next, a mold was placed on top of the substrate, with gaps that were to be filled with the magnet. In (c), the magnetic resin/paste was placed on the substrate and finally, in (d), the mold was taken away leaving only the magnet.

The key thing to note in this method is that the resin magnet mix was a room curable epoxy. Generally, when created powdered bonded magnets, the magnet needs to be heat cured and pressed. But this experiment shows promise that eventually we can make a weak magnet that needs no pressing and minimal curing.

Thus, this is extremely advantageous in that no heat treating or pressure are needed in order to obtain the final magnet. The hysteresis loop of this magnet can be seen below.

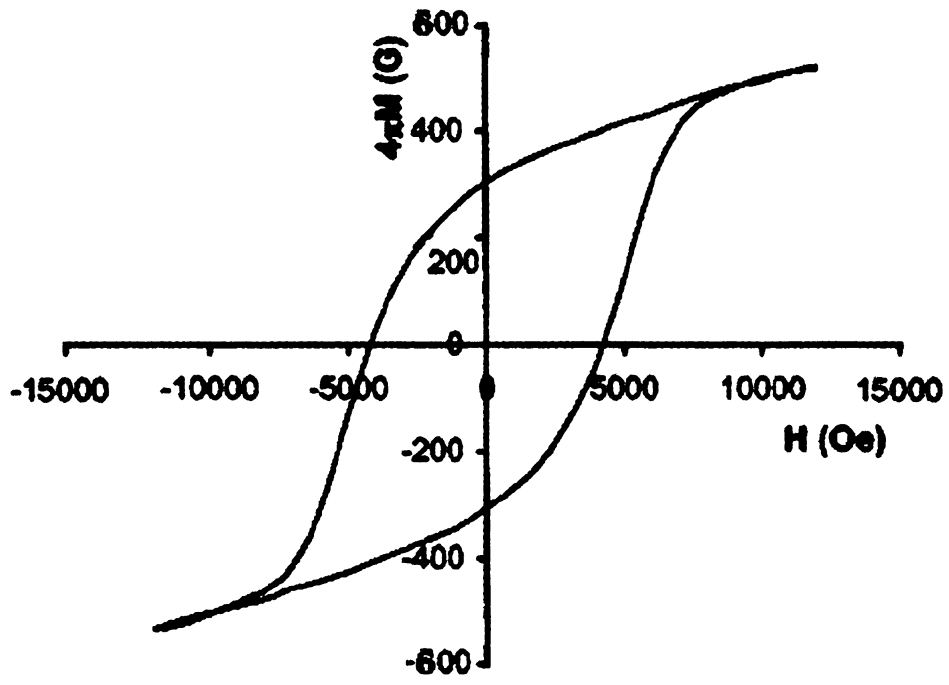

Figure 33. Hysteresis loop of the micro bonded magnet.[5]

This loop shows the magnetic characteristics of the micro bonded magnet. When being used in the application the composite impeller, the film on each of the carbon ribbons could essentially be considered a micro-bonded magnet.

In our design, we can use a simple way to model a magnet obtained this way. First of all, we know that the magnetic layer will be a mix of magnetic powder, epoxy, and carbon fibers. So, we can model it as essentially a weak magnet with perhaps a small fraction of the residual induction a pure magnet would have. The value would be at best an educated guess and estimate.

The next primary concern is how to magnetize the magnets such that they can be used for our application. This is an extremely difficult process, given the way the impeller is wound.

In [13], a method was described in which nanoparticle polymers were induced by an electric field. Although this was not used to magnetize the composite, it could be used as a stepping stone as a method for magnetizing the resin powder.

In the experiment, the carbon nanotubes were in an epoxy resin and were induced in an electric field. This was used to increase the strength of the composite. The curing method used a permanent magnet and a mold seen below.

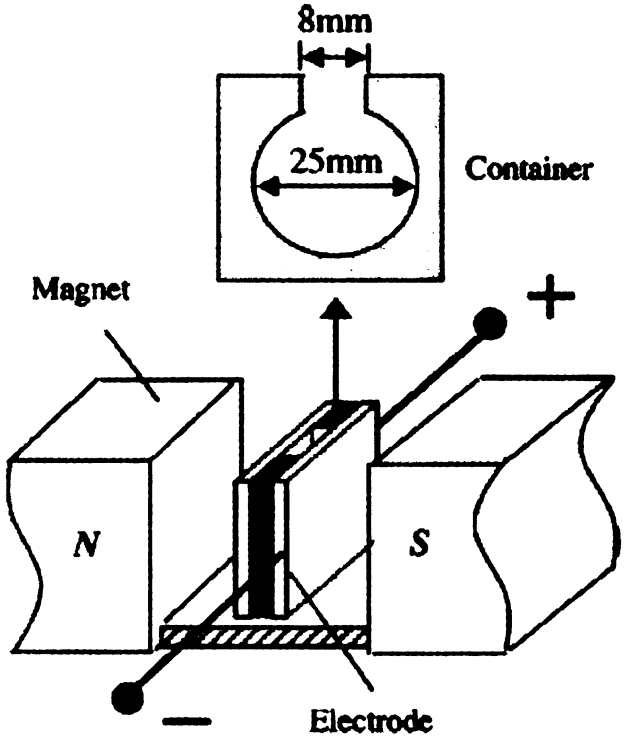

Figure 34. Mold Alignment and Curing.[13]

This diagram shows the mold used. The epoxy resin and nanoparticle mix was placed into the mold at the top. This mold was then placed between the permanent magnets seen below, and allowed to cure for 24 hours. The end result was a small wafer with its particles aligned.

The biggest problem with this experiment is that particles were not magnetized, only aligned. Also, the curing time for this experiment (hours and not seconds), is a drawback to our process. But, this shows that an epoxy nanoparticle mix can indeed be aligned using a permanent magnet.

For our purposes, this could mean that a ribbon, with epoxy/resin/magnet coating on it, could be pulled through a magnetic field device like the one seen above and be magnetized in this manner. The end result would be a wound impeller with multiple magnets on it.

These two experiments together both show that the process of magnetizing the carbon fiber ribbons is possible. First we showed that a magnetic powder resin mix can be formed on a substrate and second we showed that an epoxy nanoparticle mix can be aligned using a permanent magnet. Perhaps by using a powerful electromagnet, we can more quickly align the magnetic particles in the resin and obtain a relatively strong magnet. An important factor to note, is that the flux to density ratio of this will be the worst. Because this magnet does not exist, we will arbitrarily assign it a flux *Br* of .1T, and a density of 4900 kg/m^3.

General Motor and High Speed Considerations

When looking at the thickness of the magnets, figure 35 from [12] is extremely helpful. The chart shows flux densities for an air cored Halbach arrayed rotor and how it relates to pole pair numbers. On the chart, the value R_r is analogous to the nomenclature R_m used in this paper. For a high-speed low-torque motor, (3 or 2 pole pairs), the most desirable designs on the chart have a small rotor to magnet radius ratio. With the design here (in which we have a large rotor, and a small magnet layer), this is not feasible and the values are likely to be in the lower flux regions on this chart. Figure 36 shows the flux density with an iron core. At low pole pair numbers the chart shows that the flux density is much higher for all radius ratios. This shows that maybe even a thin layer of back iron inside the magnet ring could increase the flux density if necessary.

Basically, with an air cored rotor (such as ours), the flux density is very low for low pole pair numbers. We need to make sure we have a relatively thicker magnet layer to ensure that our design has ample flux.

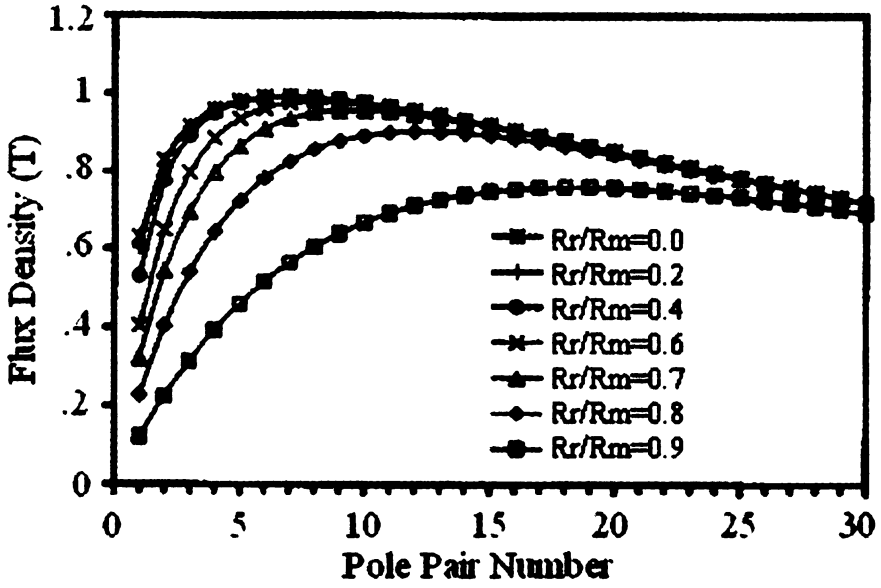

Figure 35. Flux density variation for varying magnet thickness in a Halbach array with an air cored rotor.[12]

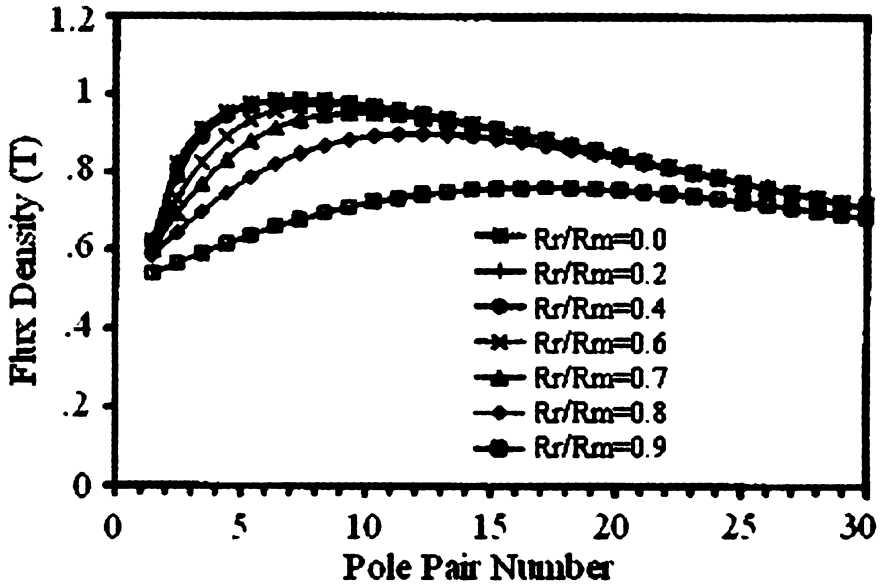

Figure 36. Flux density variation for varying magnet thickness in a Halbach array with an iron cored rotor. [12]

Another important issue in the design of a high speed motor is the wiring in the stator. The wiring used will be a copper wire. The sizing of copper wires is standardized and called the American Wire Gauge (AWG). The AWG assigns a value to different

wire thicknesses. For example, No. 10 AWG corresponds to a wire 2.989mm in diameter. As the number increases, the wire thickness decreases. The following table shows some wire gauges that are used in the spreadsheet for this project.

Table 3: Wire Gauge Sizes

AWG	diameter (mm)
Copper 0	9.53
Copper 01	8.487
Copper 02	7.558
Copper 04	5.994
Copper 06	4.753
Copper 08	3.77
Copper 10	2.989
Copper 12	2.371
Copper 14	1.88
Copper 16	1.491
Copper 18	1.182
Copper 20	0.938

These are present in a drop down menu on the spreadsheet. All of these wires will have the same resistivity ρ, which will be 1.7*10^-8 Ohm*m.

MOTOR DESIGN SPREADSHEET USER'S GUIDE

Supplementing this thesis is a spreadsheet that was used to obtain all of the results. The spreadsheet followed the equations listed earlier and calculates all the needed values in a systematic manner.

The most difficult thing to implement into the spreadsheet are loss calculations. Many losses can only be calculated using the finite element analysis and other intensive calculations.

The other most important thing regarding the spreadsheet is the weight calculation. This is a rough estimate and uses the methodology explained earlier.

So, the spreadsheet aims to quantify the final efficiency of the given design, the dimensions of the final design and the weight. These output values are intended to be used with other considerations (Halbach arrays, retaining sleeves), in order to obtain a design matrix that systematically determines the best design for this application.

First, the spreadsheet has a list of parameters that can be varied in the design, they are:

1. Number of Magnets
2. Current in Wiring
3. Magnetic Material Properties (Residual Induction, density)
4. Stator Material
5. Wire Gauge
6. Permeance Coefficient.

For simplification, all other parameters will be held constant. Many of these values are defined by compressor calculations carried out earlier, or are constants for motors that are widely known. To simplify changing these values, the wire gauge and magnet type are present as a drop down menu. The next diagram shows some of the motor constants.

Table 4: Design Constraints in the Spreadsheet

Design Inputs			
Number of Magnets	*Nm*	-	6
Magnet Pole Pairs	*Nm/2*	-	3
Phases	-	-	3
Total Slots	*Ns*	-	18
Current	*i*	*amps*	0.5
Stator Length	*Lst*	*m*	0.04
Air Gap Length	*g*	*m*	0.001
Material Choices			
Material Choices	-	-	01 Sin. Fe
Magnet Density	*pmagnet*	*kg/m^3*	4900
Residual Induction	*Br*	*T*	0.35
Stator Material	-	-	Iron
Stator Density	*pstator*	*kg/m^3*	7874
Tooth Saturation Density	*Bt*	*T*	1.6
Copper Wire Gauge	-	-	Copper 18 AWG
Wire Resistivity	*p*	*Ohm*m*	0.000000017
Wire Density	*pwire*	*kg/m^3*	8960
Wire Thickness	*Dwire*	*m*	0.001182
Lamination Stacking Factor	*Kst*	-	0.8
Leakage Factor	*Kl*	-	0.9
Relative Recoil Factor	*ur*	-	1.05
Permeability Free Space	*uo*	*H/m*	1.25664E-06
Reluctance Factor	*Kr*	-	1

The shaded boxes indicate areas where the value can be changed or modified. Another key feature of the spreadsheet is a plot of the motor that is dynamically obtained. As values are modified and changed, the diagram updates, which gives us a quick way to see what the motor looks like. An example of this output is seen below.

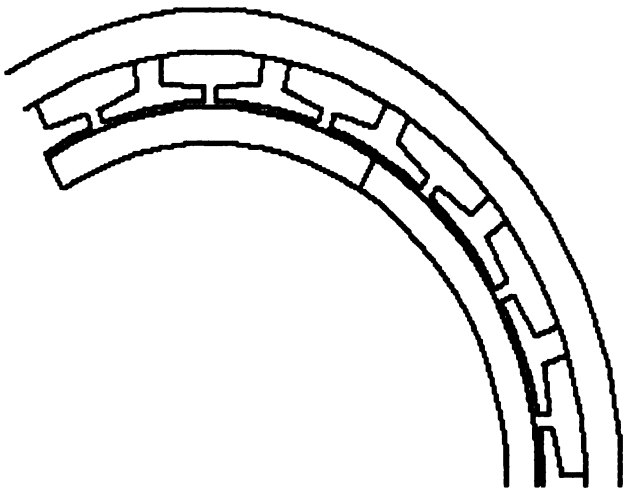

Figure 37. Dynamic Motor Diagram

The diagram only shows 2 magnet sections, and 6 stator teeth. This is constant regardless of how many magnets are actually present in the motor. The primary benefit of this diagram is showing if the motor looks "normal" and realistic. Some combinations of values give you a stator tooth that is extremely thin and centimeters long. Obviously, this cannot be constructed and common sense will dictate we must change the design.

One table in the spreadsheet summarizes some of the important data.

Table 5: Motor Final Data

			Compressor Stages			
Name	**Variable**	**Units**	**I**	**II**	**III**	**IV**
Windings	*N*	-	9	11	11	12
Back EMF	*eb*	-	488.6	533.4	580.8	633
IR^2 losses		*W*	0.00139	0.0017	0.0017	0.00186
Eddy Current Losses		*W*	21.0104	11.3575	17.2572	22.8105
Total Loss		*W*	21.0118	11.3592	17.2589	22.8124
Efficiency		%	91.3992	95.7408	94.0569	92.7923
Motor Constant	Km	-	9.05778	16.4455	14.0993	13.0654
Total Mass		kg	2.39157	3.72808	3.37402	2.72207
Slot Fill Factor			0.41947	0.72272	0.41669	0.50175

The chart shows the values for each stage and is key to our optimization. For this project the initial values such as required rotational speed, rotor torque and rotor diameter are all fixed based on previous work done. These are summarized below

Table 6: Stage Characteristics

Stage	Radius (m)	Speed (rpm)	Power (W)
1	0.05804	67222	244.3
2	0.089478	40107	266.7
3	0.074457	51240	290.4
4	0.066423	60979	316.5

These can be expanded upon by looking at how changes in the rotor radius and speed (with constant power) affect efficiency and mass.

The most important fact of any high speed motor is that losses increase as the rotational speed increases. In other words, as the rpm of the motor increases, you are fighting off losses more and more. The following chart shows how rotational speed can affect the overall efficiency for this design.

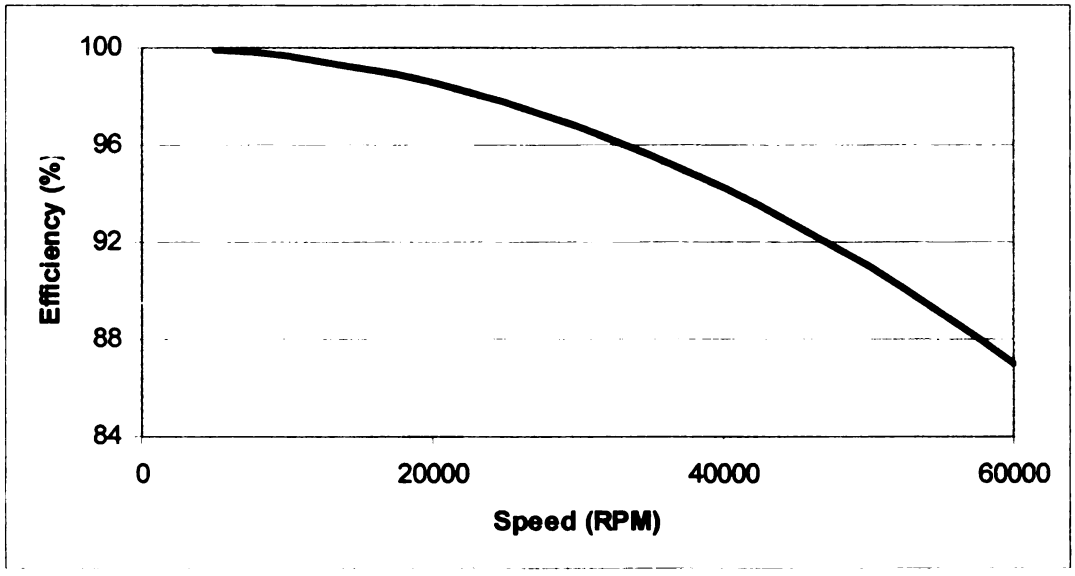

Figure 38. Efficiency Plot

This was determined for one of the stages of this compressor design. Using the data given in the spreadsheet section of this report, we can start the optimization process.

One of the design parameters we selected was the use of a Halbach array. This was to give us a more ideal air-gap flux, as well as allow us to neglect the cogging torque. By reducing the cogging torque effects, we can in turn increase the overall efficiency of the design. The spreadsheet however, does not accurately account for a Halbach array.

There will be numerous assumptions in our calculations, to summarize them, they are:

1. No back iron behind the magnetic ring
2. No Halbach Array Calculation
3. No Cogging Torque
4. No retaining sleeve present over the magnets
5. Efficiency calculations omit Core Losses
6. Modified Winding Method

First, we can look at the sintered ferrite magnet. We can optimize this by finding the highest motor constant, the highest efficiency, or the lowest weight. These can be found by crawling through the wire thicknesses, adjusting the air-gap and changing the magnet thickness via the permeance coefficient. The current will be held at .5 amps.

First, we can choose different wire types. The wires will be wound and stacked using the method explained earlier and shown in figure 19. The following plot shows how wire gauge affects the efficiency.

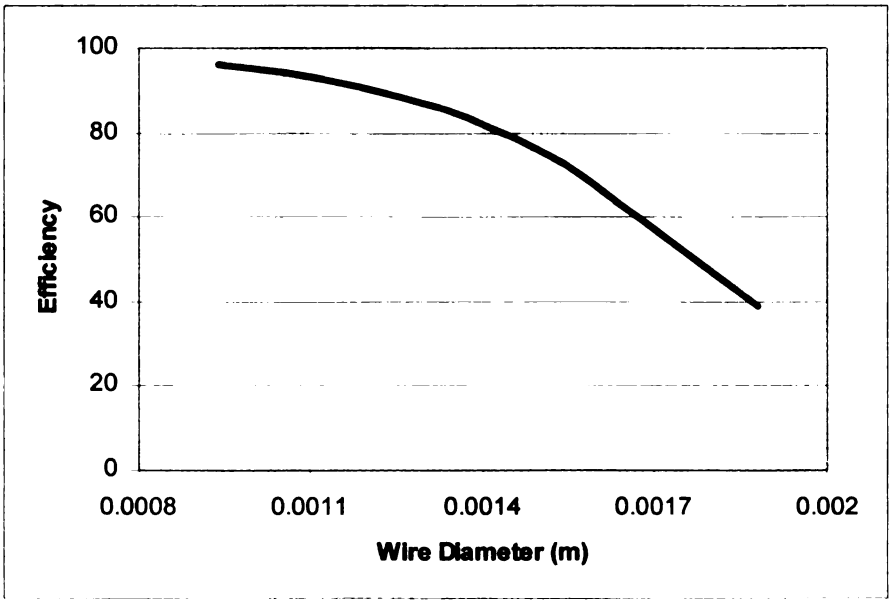

Figure 39. Efficiency Vs. Wire Diameter

This chart shows that for a simple calculation, a smaller wire gauge will lead to fewer losses in our eddy current and copper wire losses. Because our wires are relatively short, the losses due to the internal resistance in the wires are negligible. Having a thinner wire makes more sense due to the way the device will wound. However, this device has a high electrical frequency which can lead to losses in smaller wires.

As a simple solution, picking the wire with a diameter of .001182m (Wire Gauge 18), gives us both a high efficiency. Picking too small a wire gives us a winding scheme in which all the windings take place in 1 row, which isn't practical.

Using the spreadsheet we can input all our initial values and vary the permeance coefficient to see how it affects the efficiency, mass and motor constant. We will be looking at a design with 6 magnets and 3 magnet pole pairs, as well as comparing it to a 4-magnet 2-pole pair solution. The following 3 charts show this data for a ferrite magnet.

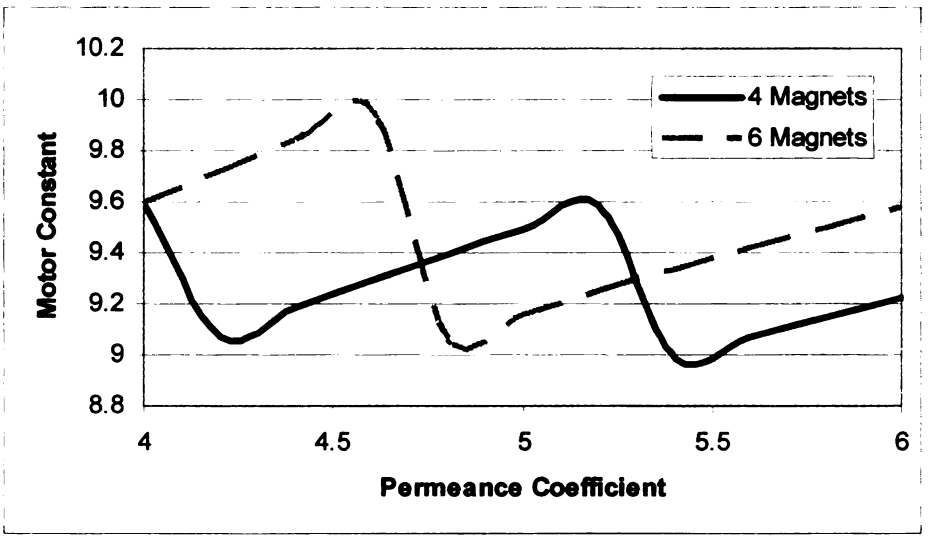

Figure 40. Motor Constant vs. Permeance Coefficient, Ferrite Magnet

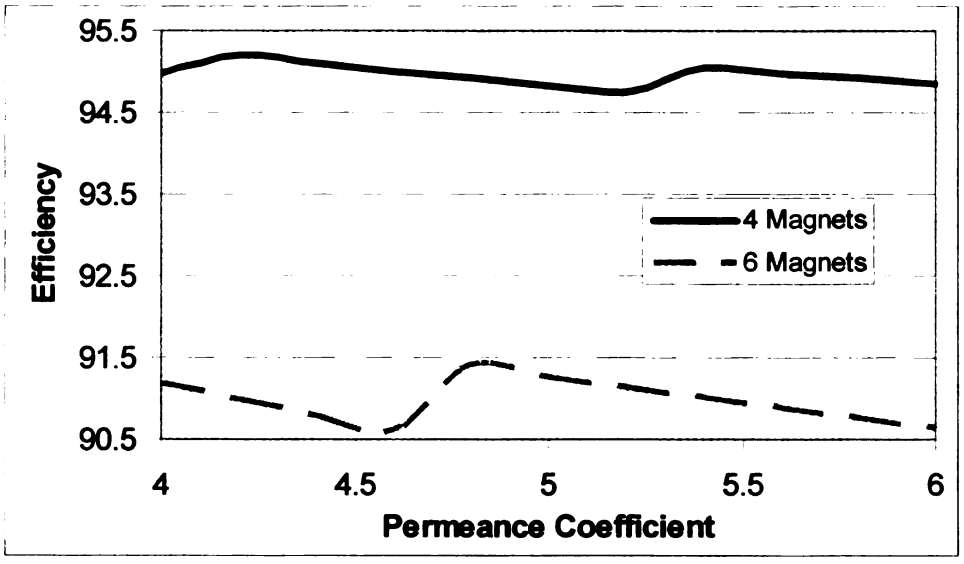

Figure 41. Efficiency vs. Permeance Coefficient, Ferrite Magnet

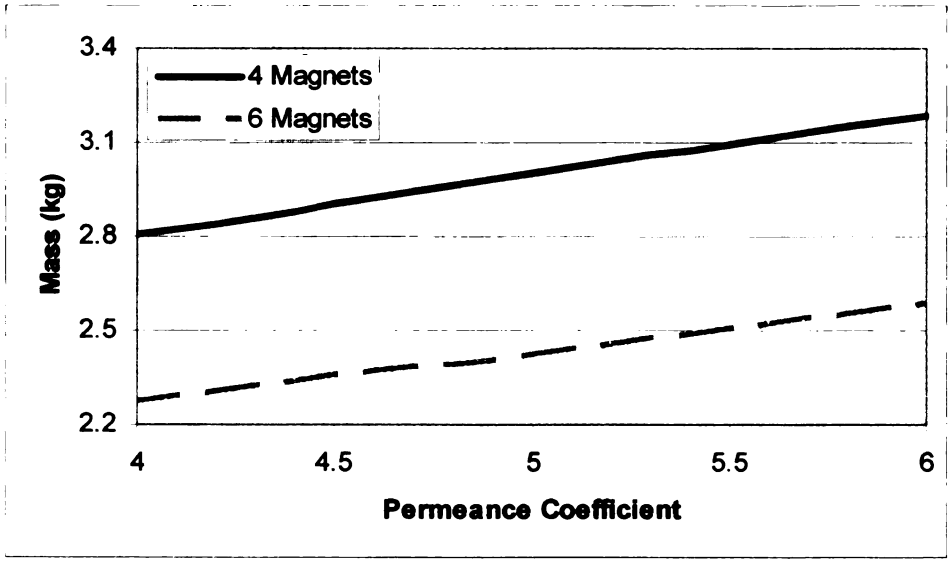

Figure 42. Mass vs. Permeance Coefficient, Ferrite Magnet

In general, these charts show that for two designs with the same magnet thickness (permeance coefficient), the 4 magnet design has much more mass. Thus, a thinner magnet ring is needed in order for a 4 magnet design to be on par with the 6 magnet design. This thinner magnet ring comes with a trade off of more windings needed. The

second chart shows that the optimum permeance coefficient for this ferrite magnet motor with these input condition is at 4.8. Permeance coefficient should be from 4 to 6 and is visible in figure 11.

The sudden jumps present in the graphs has to do with the way the winding scheme works out (as visible in figure 19) and corresponds with 1 less winding being needed due to the amount of magnets present. The following graph can outline this better.

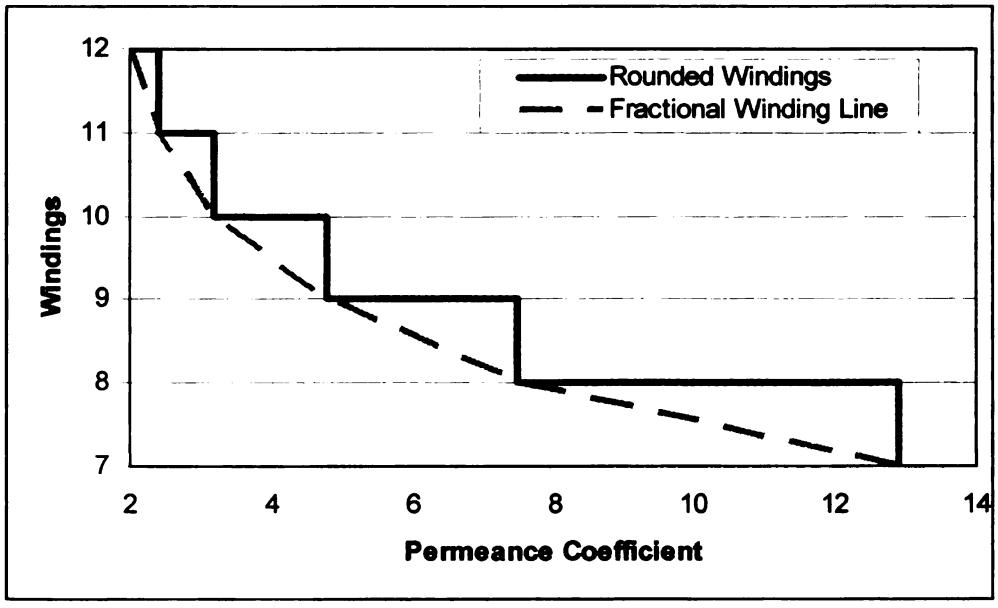

Figure 43. Windings Needed for a Ferrite 6 Magnet Motor

This stair step pattern occurs due to the fact we cannot have fractional windings in the design. Similarly, we can use this data to find the slot fill factor. This is using the winding scheme mentioned before, where windings are arranged in simple rows.

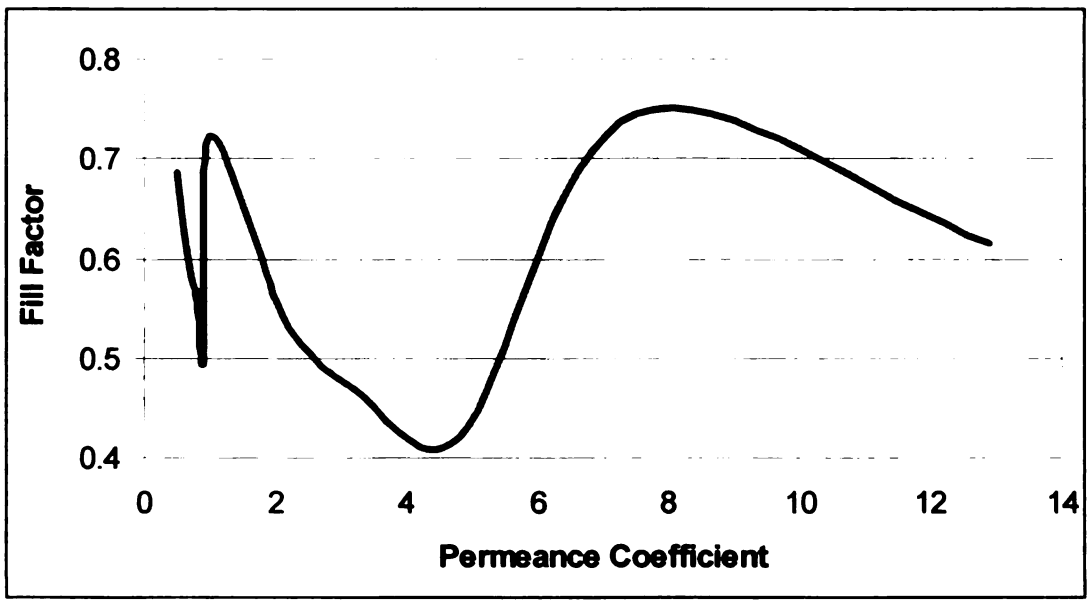

Figure 44. Fill Factor vs. Permeance Coefficient

The max points on this graph occur when a winding row is completely filled. By adding one more winding, the entire stator has to get bigger (larger diameter), in order to accommodate this extra winding. Of course, this represents a winding method that would not be seen in normal practice and also omits the fact a human hand will be winding the machine. However, it outlines how important the fill factor is. This slot fill factor chart can be created for multiple wire diameters. By keeping in mind that the permeance coefficient must be from 4-6, a chart that integrates varying wire diameter, fill factor and permeance coefficient can help ensure the slot fill factor is maximized.

Using this constrained view we can run through quick calculations on all the different magnet types. This was accomplished by varying the permeance coefficient from 4 to 6, and seeing how efficiency, motor constant and mass change. The permeance coefficient value presented represents a reasonable slot fill factor as well as the highest efficiency. This table constitutes the first run through of the data and will aim to narrow

down the magnet choices. This table represents the first stage of the compressor, and all of these have 18 wire gauge, .5 amp current and 6 magnets.

Table 7. Optimum Design Characteristics

	Permeance Coefficient	Efficiency (%)	Motor Constant (k)	Mass (kg)
Sin. Fe	4.8	91.40	9.058	2.392
Sin. NdFeB	4	65.34	9.866	4.594
Bonded NdFeB	5.6	87.31	8.966	2.832
Sin. Alnico	5.6	80.30	8.966	3.486
Bonded Alnico	4.8	91.40	9.058	2.450
Sin SmCo	4	74.94	9.866	3.639
Bonded SmCo	4	86.57	9.044	2.607
Magnet Paste	4	97.70	9.044	2.478

These values can be put into a weighted design matrix, in order to determine the best possible design solution.

Table 8. Weighted Design Matrix

	Cost	Weight	Efficiency	Motor Constant	Temp. Stability	Total
Weighting	**10**	**5**	**5**	**5**	**5**	30
01 Sin. Fe	10	4	4	2	1	21
02 Sin. NdFeB	3	1	1	5	4	14
03 Bonded NdFeB	1	4	3	3	4	15
04 Sin. Alnico	7	2	2	1	3	15
05 Bonded Alnico	5	4	4	2	3	18
06 Sin SmCo	3	2	2	5	5	17
07 Bonded SmCo	1	3	4	1	5	14
08 Magnet Resin	7	4	5	1	1	18

This design uses a few categories to help find a solution. First, cost basically looks at how much the magnet is to create, or in the case of the magnetic paste, how expensive the technology might be to implement. Weight, efficiency, and motor constant were all obtained from the spreadsheet optimization. Temperature stability looks at how well the magnets can cope with high temperatures, but also how easily they degrade

when present in higher temperatures. The discussion earlier in the magnetics section was used to come to these values.

From this simple analysis, the ferrite magnet comes out with the highest score. Although earlier it was mentioned that high speed motors generally favor rare earth magnets, the biggest reason why a ferrite would be better is that we are not making a design that requires large torque. Also, this calculation was carried out with a relatively low current. Another choice that is noteworthy to look over is the magnetic resin solution. Again, this solution modeled the magnetized shroud/resin mix as an extremely weak magnet.

Also, these calculations were created with 3 magnet pole pairs instead of 2. Generally high speed devices use only 1 or 2 magnet pole pairs, in order to keep the cost of the frequency drive down. It is possible that by having such a large radius, the design might not work as well due to the magnets being too big and spanning too large of an arc length.

These next set of plots will use a constant tip speed. We will assume a rotor of radius 5cm, spinning at 60,000 rpm. For these numbers, it works out to a tip speed of 314.15 m/s. As we increase the radius, the rotational speed will slow down to maintain the constant tip velocity. This can give us an idea as to how radius will affect the motor design. First, let's look at the mass of the motor with a 6 magnet ferrite magnet, and compare it to a plot of the magnetic resin.

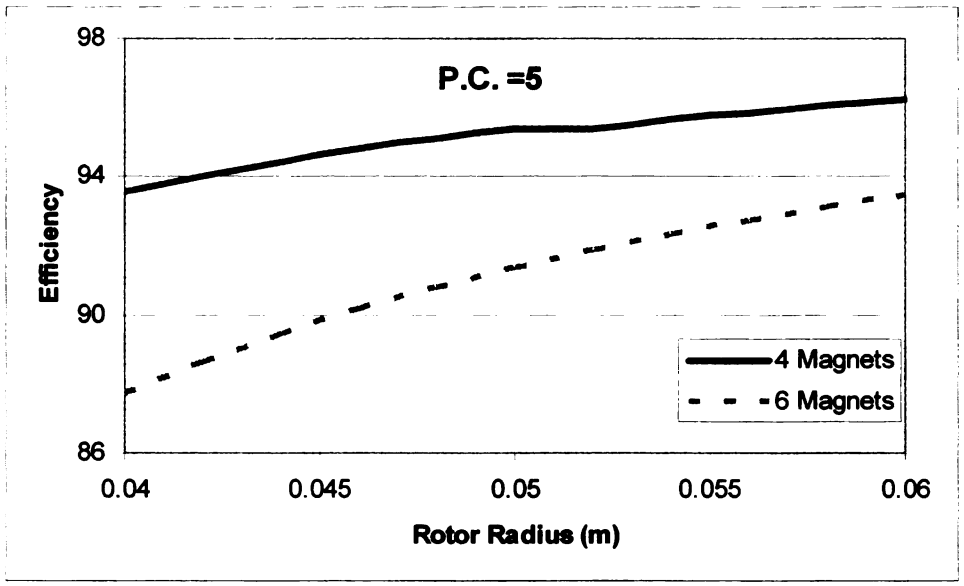

Figure 45. Efficiency vs. Rotor Radius for a Ferrite Magnet

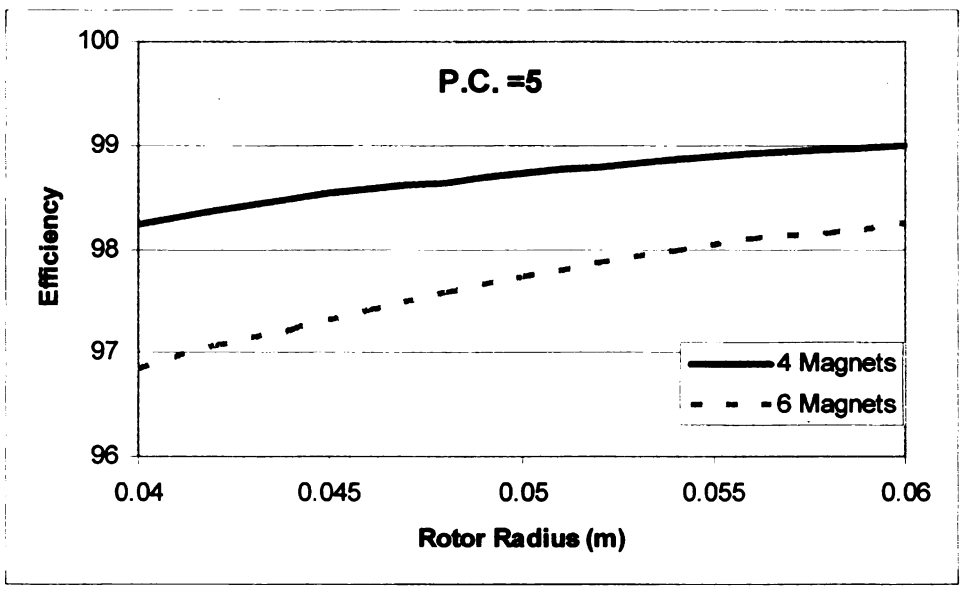

Figure 46. Efficiency vs. Rotor Radius for a Magnetic Resin Array

These plots show a permeance coefficient of 5. It shows that the efficiency of a 4 magnet motor is higher than a 6 magnet motor when the magnet thickness is held constant. Also, as the rotor radius increases, the efficiency increases as well. Also, the

magnetic resin has a higher overall efficiency for a given rotor radius. The next set of plots will show the mass of the motor.

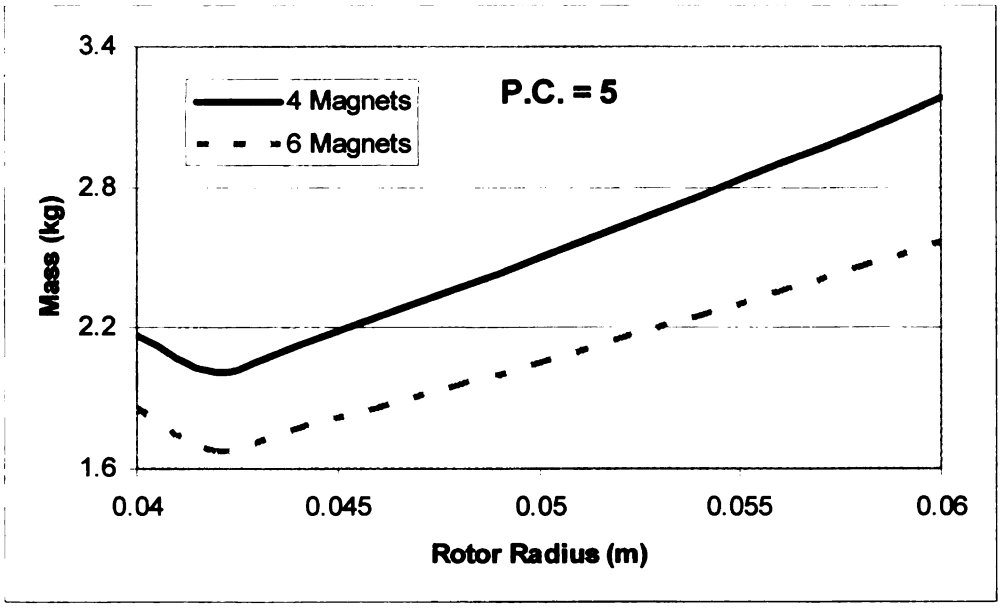

Figure 47. Mass vs. Rotor Radius for a Ferrite Magnet

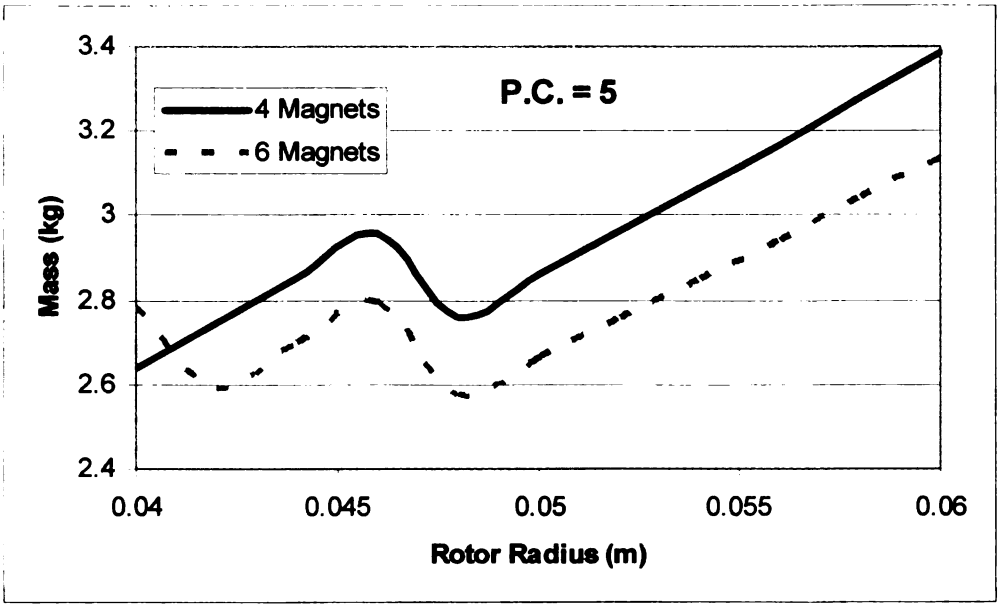

Figure 48. Mass vs. Rotor Radius for a Magnetic Resin Array

The first ferrite plot shows that the mass increases as the rotor radius increases. The second plot shows more of a saw pattern. This occurs due to the fact the stator for the magnetic resin requires many more windings. Thus, by increasing the rotor radius, you are increasing the circumference of the motor at the slot opening. This in turn means that as the rotor radius increases, more windings can fit across in a row. This stair step pattern takes a dip when a row is eliminated by the increasing radius. Since the ferrite magnet has less windings, however, this occurs much less frequently. Also, at lower rotor radius the ferrite magnet is lighter. As the rotor radius increases the magnet resin approach has less mass.

For the preceding rotor radius calculations, we kept the tip speed constant. Now, we can see how increasing the tip speed will affect the design.

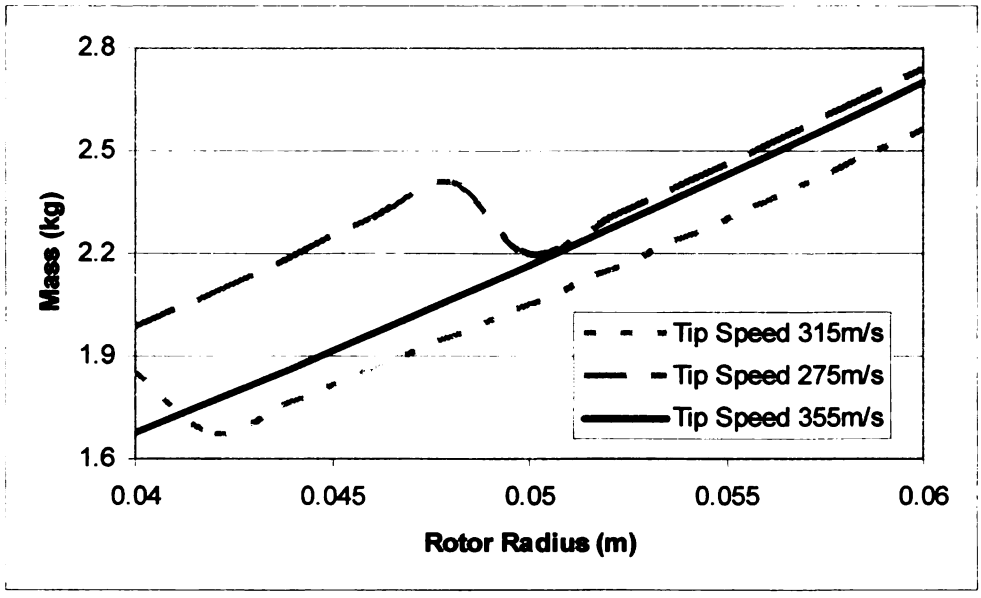

Figure 49. Mass vs. Rotor Radius for a Ferrite Magnet

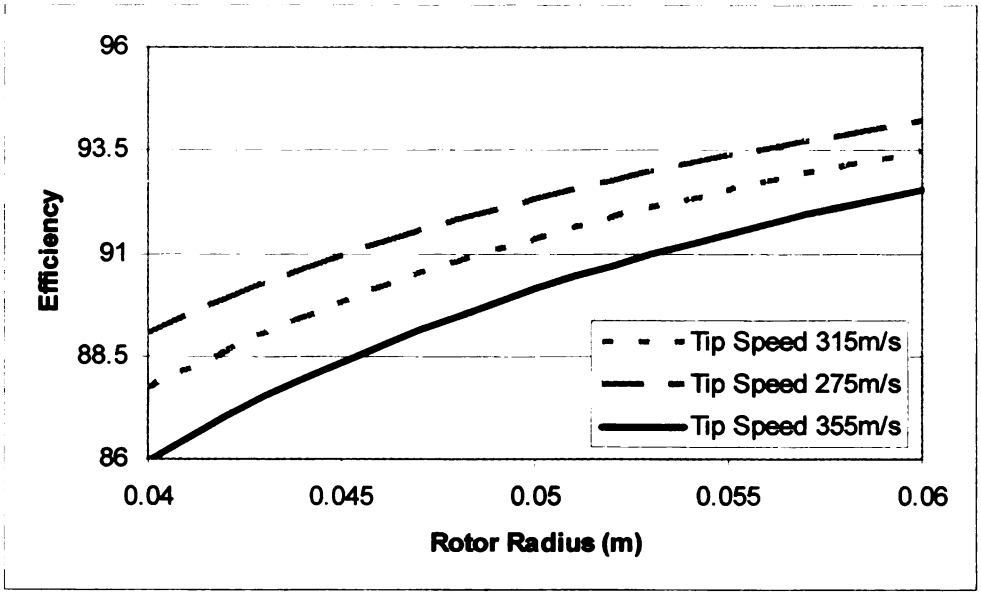

Figure 50. Efficiency vs. Rotor Radius for a Ferrite

By increasing the tip speed you are increasing the angular frequency. This increase in angular frequency causes our efficiency calculation to decrease. Another thing that a higher tip speed does is decrease the torque from equation 11. Since angular frequency is equal to the tip speed divided by the radius, with a constant power the torque will go down. A lower torque means that less windings are needed, thus the mass will be less. The mass plot shows this in a way. The sudden dips are places where a winding row is eliminated. Although the 355m/s plot isn't the lowest for the range shown, over the long run, it will have much lower mass. This decrease in mass is not without a cost. Increasing the tip speed at constant radius increases the angular frequency, which increases the cost of the frequency drive needed to run the motor. Using equation 11, and rearranging, we obtain the following equation:

$$T = P * \frac{r}{V} \tag{42}$$

This simple relation can tell us how velocity and power affect the torque and thus the overall motor. Increasing the power by a factor of 2 is the same as decreasing the velocity by a factor of 2. It is very easy to relate these parameters together.

Next, we can look at how changing the current can affect mass and efficiency. All of the following plots were calculated at a permeance coefficient of 5.

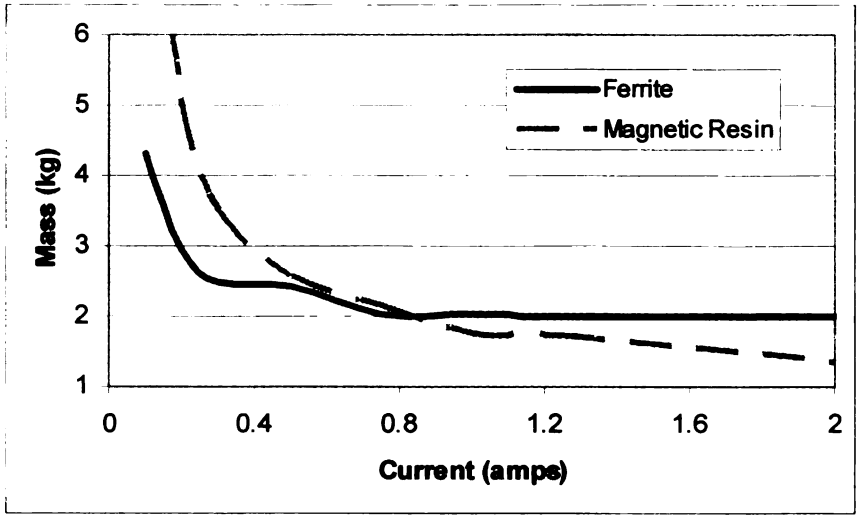

Figure 51. Mass vs. Current for a Magnetic Resin and Ferrite

This plot shows that for lower current values the magnetic resin has a much higher mass. However, as the current is ramped up this becomes much lighter than the ferrite. At higher currents, the masses will tail off as the number of windings slowly reduces to 1 winding.

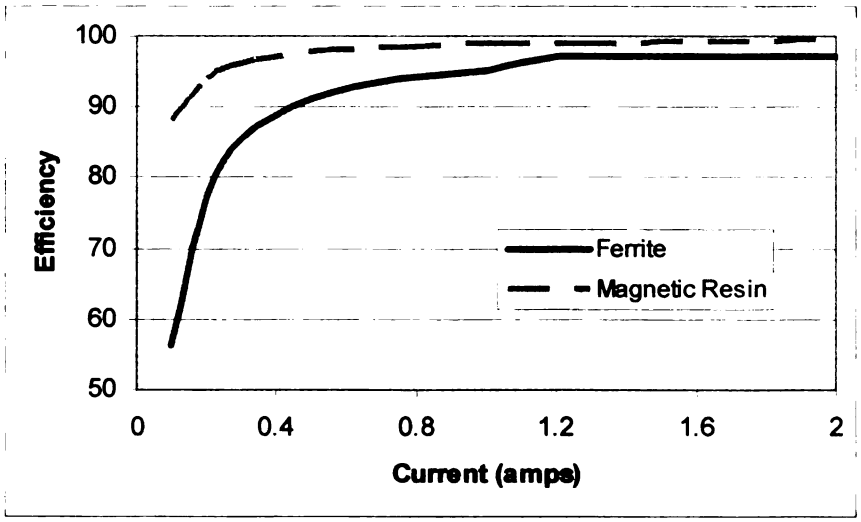

Figure 52. Efficiency vs. Current for a Magnetic Resin and Ferrite

This figure shows how efficiency greatly increases as the current increases. For any design the current should be kept high to minimize losses. The magnetic resin has higher efficiency for a given current.

The preceding plots and also the plots in the appendix can give us a good idea as how to factors vary and can affect each other. Using some of this information, we can begin to find the best design. The current will be purposely kept from .5 to 1 amps. This best design will look at a ferrite magnet.

In figure 45, it shows that for a 4 magnet motor the efficiency is always much higher. A 4 magnet motor also has the advantage of driving down the cost of the frequency drive. Since we are dealing with such high speeds, driving down the electrical frequency is beneficial.

This means however, that the mass of the design will be much higher compared to a 6 magnet motor (with a fixed permeance coefficient). Since we want to keep the air-gap constant, this means to have a competitive mass, we need to use the lower end of the

permeance coefficient to obtain a thinner magnet ring. This trade off means we'll have less air-gap flux (based on figure 11). The biggest problem with only 4 magnets is the size of the slot. Since or rotor is relatively large, too few magnets will mean the slot size will be too big. A thinner magnet also means that we'll require more windings. More windings can be counterbalanced by more current if necessary. However, because of the low torque requirements for this motor the number of windings should be still easy to manage.

We should also keep figure 44 in mind and recognize we need to maximize the slot fill factor. Using this information and the spreadsheet we can come up with a preferred design. Due to the fact each stage has its own power, radius and rotational speed requirements, the optimization will be carried out 4 times.

The optimization will utilize the assumptions explained earlier and will use the data already presented. The following figure shows what the final motor will look like.

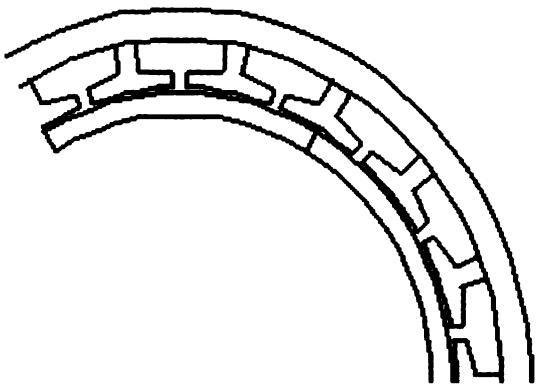

Figure 53. Final Motor Values

This table will show what the various motor dimensions are, as well as what the key characteristics are.

Table 9. Final Design Summary and Characteristics

Dimension Summary						
			Compressor Stages			
Name	**Variable**	**Units**	**I**	**II**	**III**	**IV**
Rotor Radius	*Rr*	*m*	0.05804	0.08948	0.07446	0.06642
Magnet Radius	*Rm*	*m*	0.06284	0.09408	0.07946	0.07042
Air-Gap	*g*	*m*	0.001	0.001	0.001	0.001
Magnet Length	*Lm*	*m*	0.0048	0.0046	0.005	0.004
Stator Inner Radius	*Rs*	*m*	0.06384	0.09508	0.08046	0.07142
Width Stator Yoke	*wsy*	*m*	0.00664	0.00987	0.00846	0.00719
Stator Yoke Inner	-	*m*	0.07211	0.10099	0.08873	0.0797
Stator Outer Radius	*Rso*	*m*	0.07876	0.11086	0.09719	0.08688
Width Slot Opening	*wso*	*m*	0.00236	0.00236	0.00236	0.00236
Bottom Slot Width	*wsb*	*m*	0.01992	0.03082	0.02572	0.02257
Shoe Tip Depth	*dsh*	*m*	0.00236	0.00236	0.00236	0.00236
Shoe Taper Depth	*dt*	*m*	0.00118	0.00118	0.00118	0.00118
Windable Slot Depth	*ds*	*m*	0.00473	0.00236	0.00473	0.00473
Width Tooth Body	*wtb*	*m*	0.00443	0.00658	0.00564	0.00479
Tooth Head Width	-	*m*	0.01992	0.03082	0.02572	0.02257

Motor Characteristics Summary						
			Compressor Stages			
Name	**Variable**	**Units**	**I**	**II**	**III**	**IV**
Windings	*N*	-	9	11	11	12
Back EMF	*eb*	-	488.6	533.4	580.8	633
IR^2 losses		*W*	0.00139	0.0017	0.0017	0.00186
Eddy Current Losses		*W*	21.0104	11.3575	17.2572	22.8105
Total Loss		*W*	21.0118	11.3592	17.2589	22.8124
Efficiency		%	91.3992	95.7408	94.0569	92.7923
Motor Constant	Km	-	9.05778	16.4455	14.0993	13.0654
Total Mass		kg	2.39157	3.72808	3.37402	2.72207
Slot Fill Factor			0.41947	0.72272	0.41669	0.50175

These tables give dimensions and values that can be used to create the motor needed to run the device. The rest of the data from the spreadsheet is in Appendix C.

The motor solution for this would be more efficient and have fewer losses. This is due to the fact that the electrical frequency of the motor would be lower and thus less eddy current losses would be induced. For a high speed motor, minimizing any losses is ideal. Another solution that would be noteworthy to look at is the solution that used a magnetic resin bath.

Although this is the preferred solution in the long run, currently there are too many unknowns as to how this would be implemented. The weak magnet is possible due to the low torque required in this design. This design also had the least amount of losses, and gave the lightest overall design.

Above all, the spreadsheet gives the user a good idea as to what the general dimensions, magnet requirements as well as input data are needed for the motor design. This can provide an excellent first step, when numerous design ideas can quickly be swapped.

CONCLUSION

This thesis was able to show how to create an electric motor to serve as the drive system for an impeller. This topic was discussed in the context of a high speed impeller in a chiller that uses water as a refrigerant. All of the essential background details for understanding the basic motor design were presented and explained in their entirety.

Following the procedure presented in the preceding sections gives an approximate idea of the quality and the dimensions of the motor. However, this methodology does not take into consideration numerous losses and is not adapted for Halbach arrays.

It is also very difficult to determine how the motor will behave with an impeller as the backing to the magnet. This perhaps would be similar to a device that is between an air cored rotor and an iron cored rotor, but above all, is something best left relegated to a complex finite element analysis.

In general, a simple methodology can be used to describe how the various data was crawled through using the spreadsheet. This is loosely followed, and outlines how many of the charts were explained and how data leading into the design matrix was obtained. The following flow chart shows this simple procedure

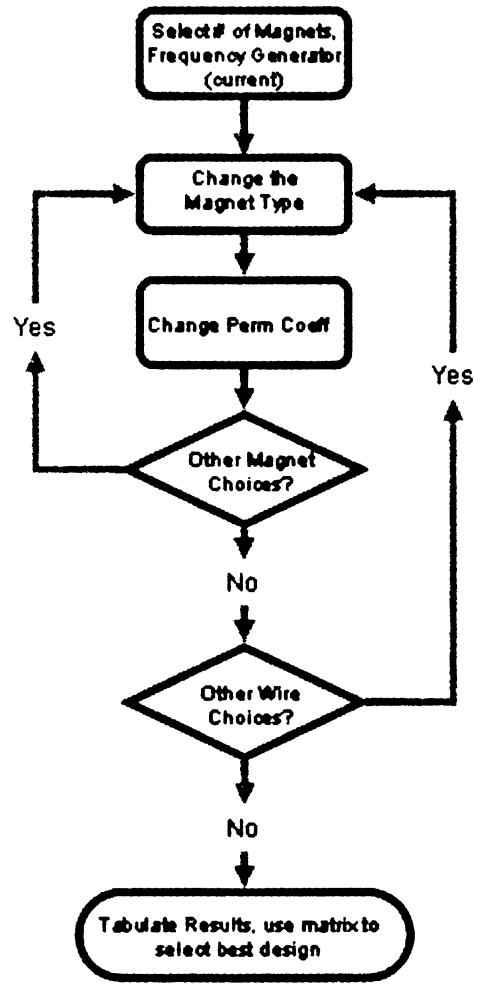

Figure 54. Procedure Flow Chart

The data obtained from this data crawling outlined a lot of important trends and key relationships. Some of these key trends presented in this thesis can be summarized in the following bulleted list:

1. Air-gap Flux tails off as Permeance Coefficient Increases, ideal range is 4 to 6
2. Higher rotational speeds have lower efficiencies and larger losses
3. Increasing the rotor radius while keeping the tip speed constant increases efficiency

4. Increasing the tip speed while keeping required power constant decreases mass and decreases efficiency
5. High slot fill factor is ideal
6. The more magnet pairs you have, the lower the mass and efficiency
7. Increasing current lowers the mass. This levels off as the current is further increased
8. Increasing the current also increases the efficiency
9. Lower pole pair numbers means a lower electrical frequency, which vastly reduces the cost of the frequency drive.
10. Better quality magnets means more efficient torque production
11. Higher residual induction generally means more mass

This list is very general and should be used with many precise calculations and a very holistic approach. As with any design process, there is no systematic way to solve every design problem.

The final design chosen was a motor with 3 magnet pairs utilizing a ferrite magnet arranged in a Halbach array. This consideration was made based on calculations carried out on a spread sheet, as well as a design matrix which was used to weigh design criteria. A separate calculation was carried out for each of the 4 stages of the device. The aim of each of these stages was to obtain a solution with low mass, a reasonable efficiency, and a high slot fill factor.

Continuing research might focus on doing a finite element analysis on the motor design presented here. This would more accurately be able to calculate losses, as well as learn about how flux travels through the design. This model could include an impeller at the center.

Further studies can be conducted into how the magnets are best integrated into the rotor and how various sleeves can affect the design. Also the particularities of magnetizing the composite impeller directly are open to investigations. An optimization for low cost and small size may be desired too.

A prototype could also be constructed. This would more adequately show how the technologies discussed might work in practice. The spreadsheet could also be upgraded to account more accurately for a Halbach array.

Another big thing to further address is the winding method. This could be looked at by creating a better winding algorithm and looking at the slot openings more closely. Also, an investigation could be carried out into whether distributed winding would be the best solution for this application.

Lastly, a comparative study can be completed that compares the merits of this innovative drive system, versus merely rotating the impeller using a motor, gear box and a shaft.

Above all this thesis was able to provide the foundation towards the design of a permanent magnet motor drive system for a compressor in a water as a refrigerant device. The thesis researched basic key concepts in the numerous disciplines required to tackle such a problem. This thesis should serve as a guide towards working towards a final design and as the first preliminary study in a long multi-step process of engineering design.

Appendix A: Winding Diagram [4]

N_s	N_m	N_{spp}	R_{ro}/R_{so}	K_m	α^*_{sk}	n_{cog}
18	6	1	0.56	0.96	1	3

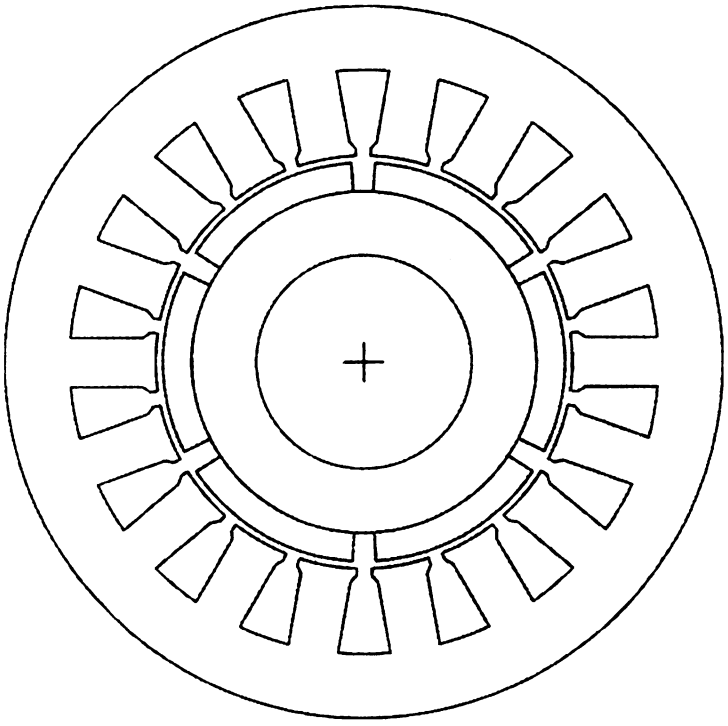

Coil No.	Coil Angle, °E	Phase A		Phase B		Phase C	
		In	Out	In	Out	In	Out
1	0	1	4	5	8	3	6
2	0	1	16	5	2	3	18
3	0	7	4	11	8	9	6
4	0	7	10	11	14	9	12
5	0	13	10	17	14	15	12
6	0	13	16	17	2	15	18
7							
8							
9							
10							
11							
12							

Figure A1. Winding Chart for 3 phase 6 magnet motor

Appendix B: Motor Plots

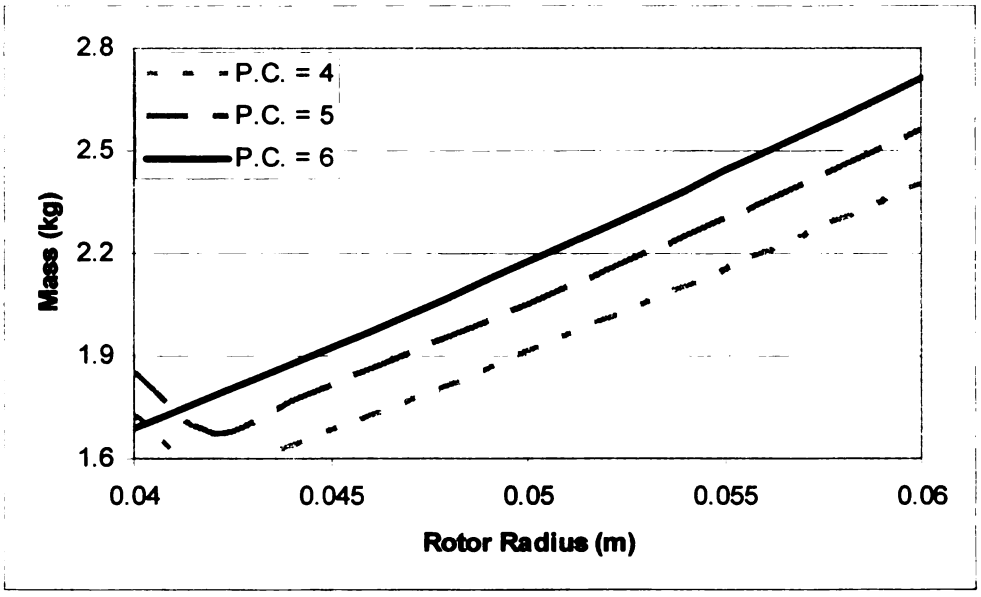

Figure B1. Mass vs Rotor Radius for a Ferrite Magnet, 6 Magnets

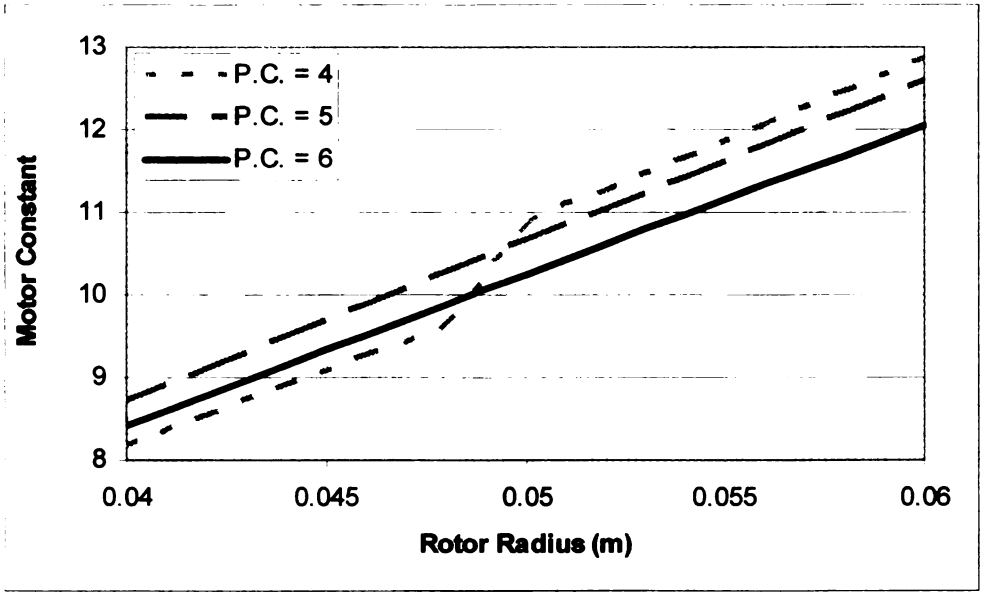

Figure B2. Motor Constant vs Rotor Radius for a Ferrite Magnet, 6 Magnets

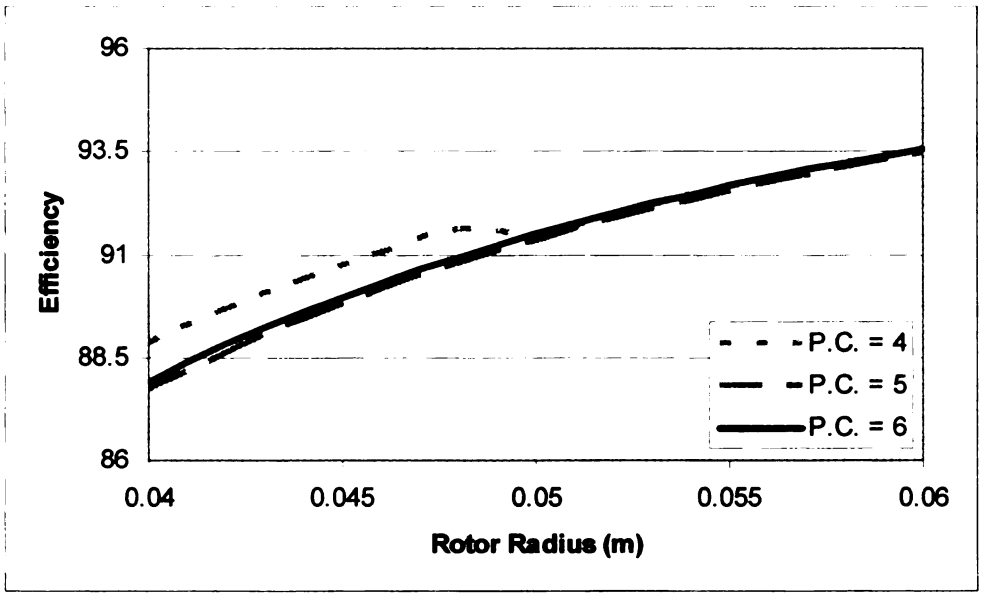

Figure B3. Efficiency vs Rotor Radius for a Ferrite Magnet, 6 Magnets

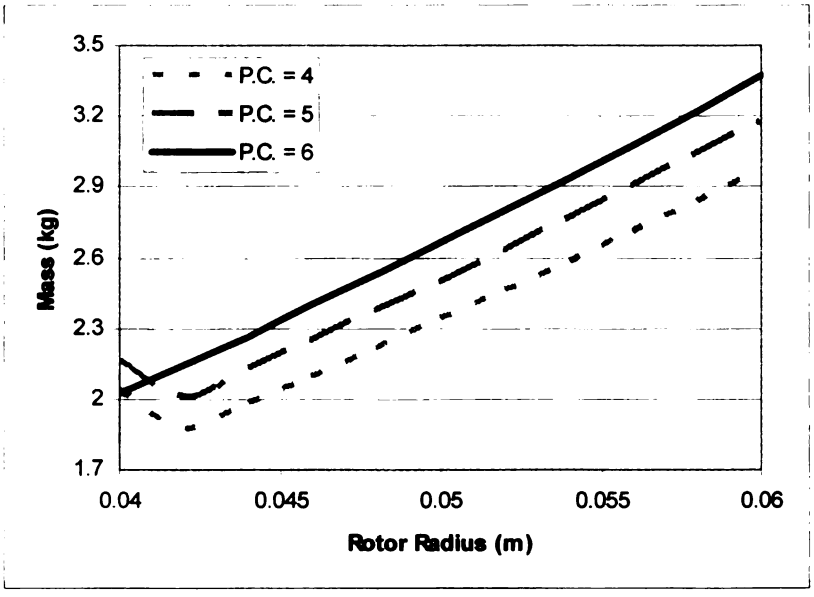

Figure B4. Mass vs Rotor Radius for a Ferrite Magnet, 4 magnets

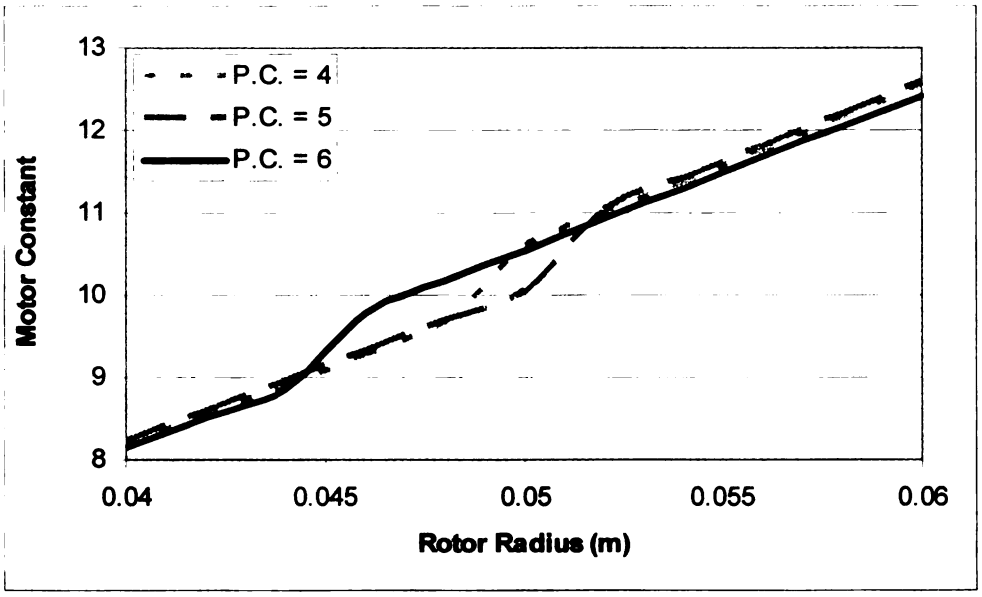

Figure B5. Motor Constant vs Rotor Radius for a Ferrite Magnet, 4 Magnets

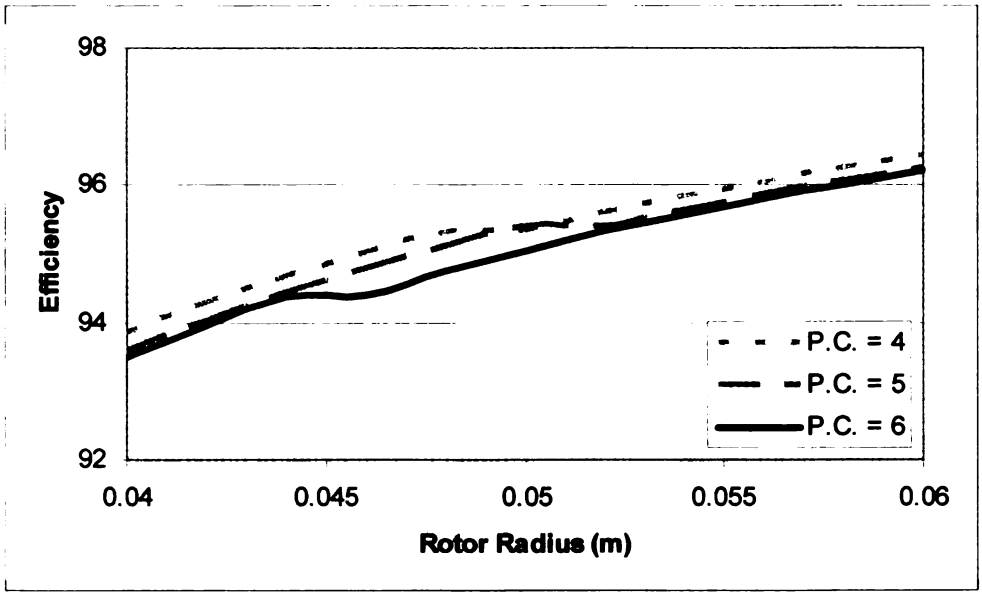

Figure B6. Efficiency vs Rotor Radius for a Ferrite Magnet, 4 Magnets

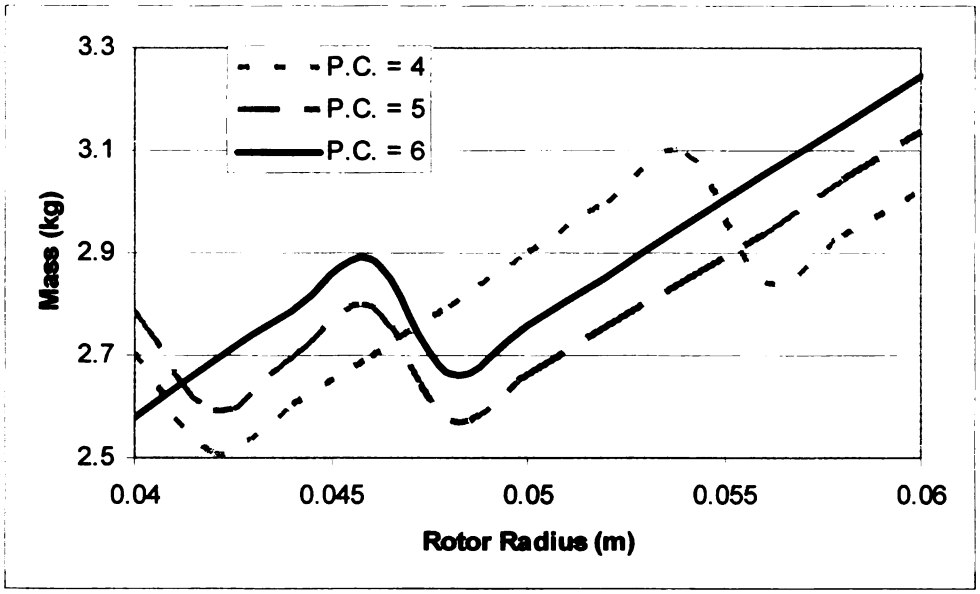

Figure B7. Mass vs Rotor Radius for a Magnetic Resin Array, 6 Magnets

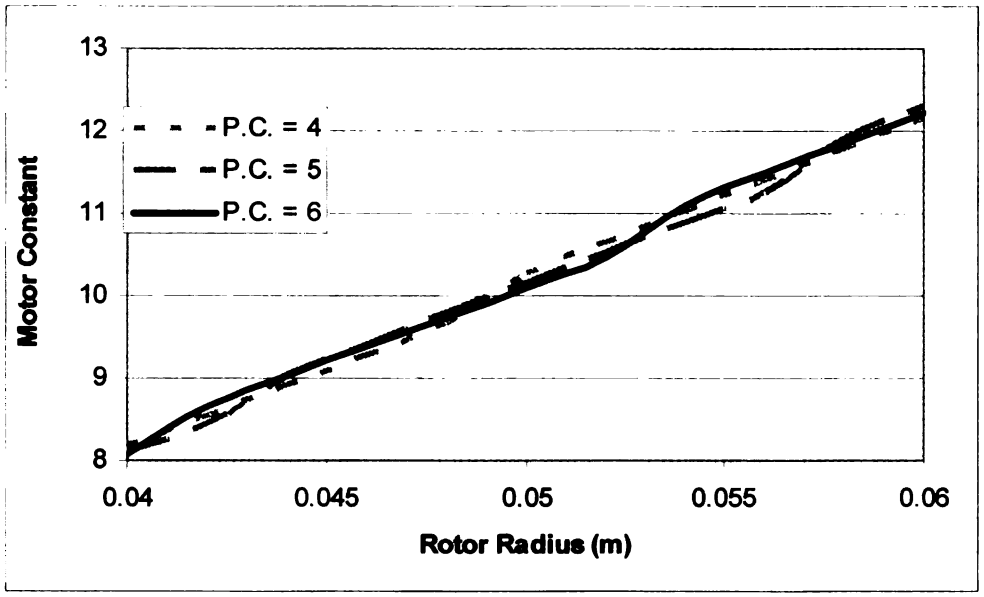

Figure B8. Motor Constant vs Rotor Radius for a Magnetic Resin, 6 Magnets

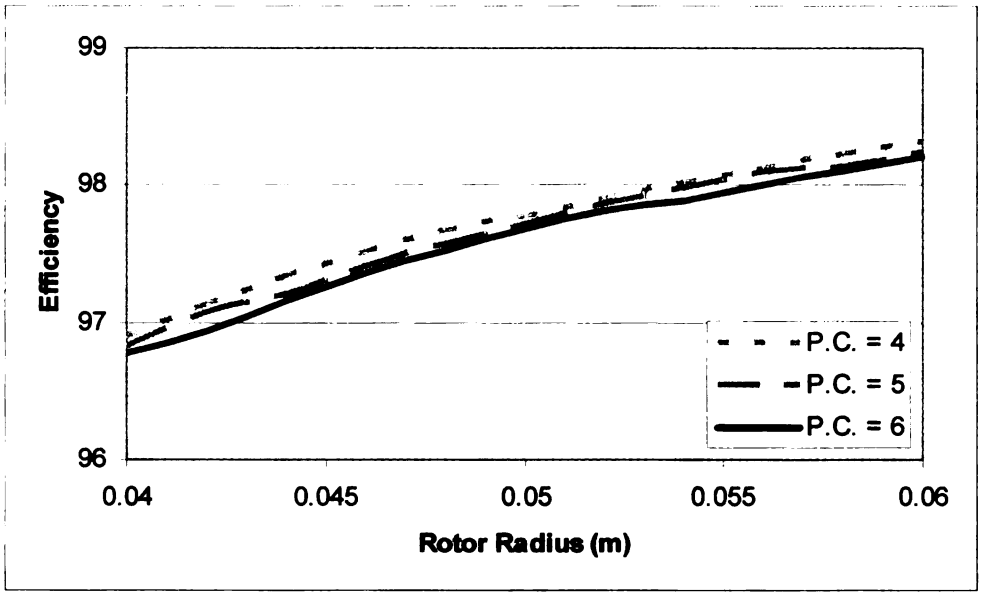

Figure B9. Efficiency vs Rotor Radius for a Magnetic Resin, 6 Magnets

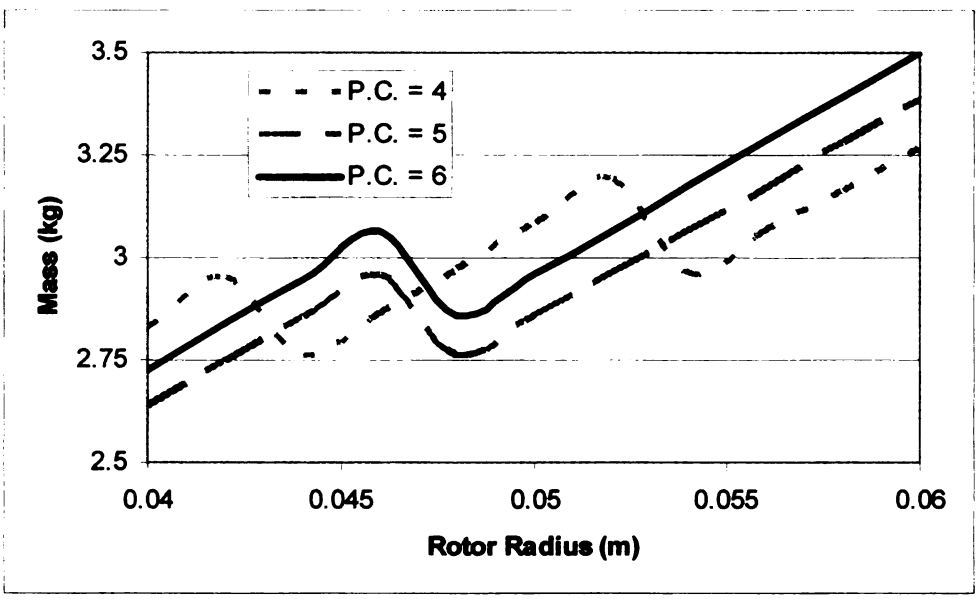

Figure B10. Mass vs Rotor Radius for a Magnetic Resin Array, 4 Magnets

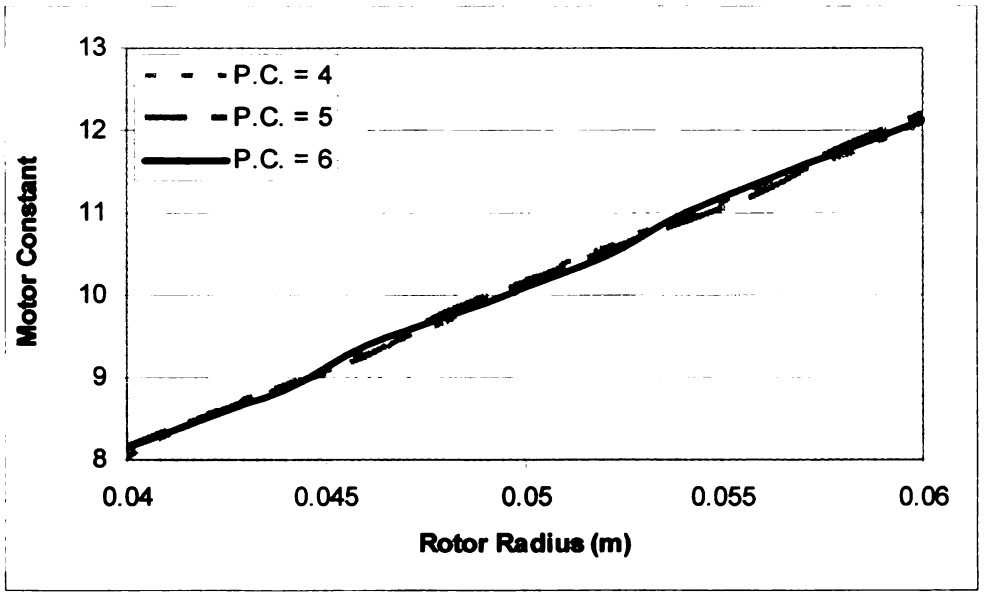

Figure B11. Motor Constant vs Rotor Radius for a Magnetic Resin, 4 Magnets

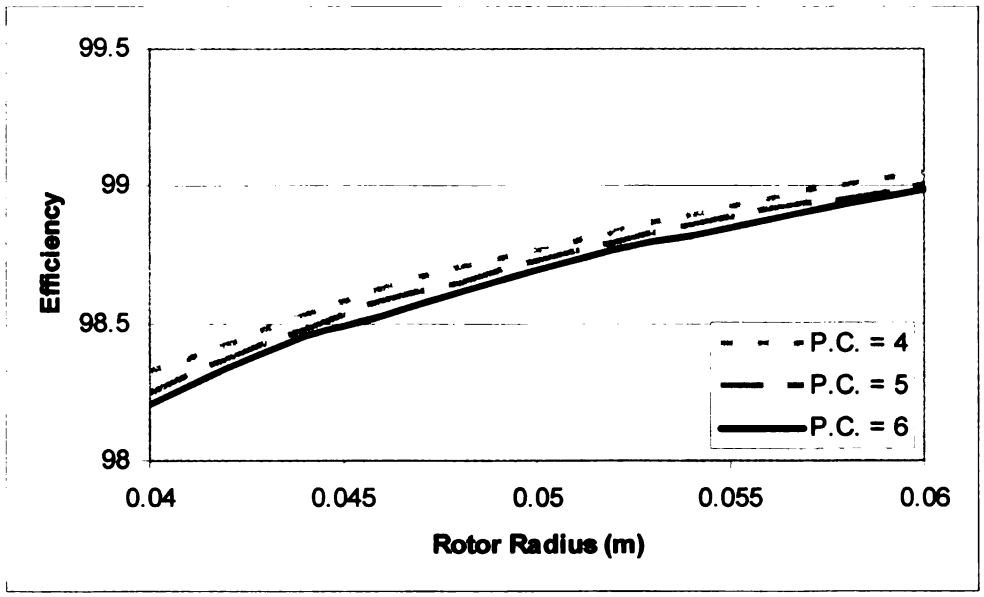

Figure B12. Efficiency vs Rotor Radius for a Magnetic Resin, 4 Magnets

Appendix C: Motor Calculations

Table C1. Final Design Inputs

Number of Magnets	*Nm*	-	6
Magnet Pole Pairs	*Nm/2*	-	3
Phases	-	-	3
Total Slots	*Ns*	-	18
Current	*i*	*amps*	0.5
Stator Length	*Lst*	*m*	0.04
Air-gap Length	*g*	*m*	0.001
Material Choices			
Material Choices	-	-	01 Sin. Fe
Magnet Density	*ρmagnet*	*kg/m^3*	4900
Residual Induction	*Br*	*T*	0.35
Stator Material	-	-	Iron
Stator Density	*ρstator*	*kg/m^3*	7874
Tooth Saturation Density	*Bt*	*T*	1.6
Copper Wire Gauge	-	-	Copper 18 AWG
Wire Resistivity	*ρ*	*Ohm*m*	0.000000017
Wire Density	*ρwire*	*kg/m^3*	8960
Wire Thickness	*Dwire*	*m*	0.001182
Lamination Stacking Factor	*Kst*	-	0.8
Leakage Factor	*Kl*	-	0.9
Relative Recoil Factor	*ur*	-	1.05
Permeability Free Space	*uo*	*H/m*	1.25664E-06
Reluctance Factor	*Kr*	-	1

Table C2. Final Design Calculations

Calculations			Compressor Stage			
Name	**Variable**	**Units**	**I**	**II**	**III**	**IV**
Stage rpm		*rpm*	67222	40107	51240	60979
Angular Speed	*wm*	*rad/s*	7039.47	4199.99	5365.84	6385.7
Electrical Ang Speed	*we*	*rad/s*	21118.4	12600	16097.5	19157.1
Rotor Radius	*Rr*	*m*	0.05804	0.08948	0.07446	0.06642
Stage Power	*P*	*W*	244.3	266.7	290.4	316.5
Stage Torque	*T*	*nm*	0.0347	0.0635	0.05412	0.04956
Magnet Radius	*Rm*	*m*	0.06284	0.09408	0.07946	0.07042
Magnet Length	*lm*	*m*	0.0048	0.0046	0.005	0.004
Stator Length	*lst*	*m*	0.04	0.04	0.04	0.04
Air-gap Length	*g*	*m*	0.001	0.001	0.001	0.001
Flux Concentration Factor	*Co*	-	1	1	1	1
Calculated Perm Coef	*Pc*	-	4.8	4.6	5	4
Back emf	*eb*	*V*	488.6	533.4	580.8	633
Air-gap Flux	*Bg*	*T*	0.25846	0.25646	0.26033	0.2495
Flux Density		-	0.73846	0.73274	0.7438	0.71287
Windings	*N*		8.90308	10.9662	10.9016	11.7533
Windings Rounded	*N*	-	9	11	11	12
Total Flux	*Ototal*	*T*	0.00408	0.00606	0.0052	0.00442
Slot Opening	*wso*	*m*	0.00236	0.00236	0.00236	0.00236
Tooth Width	*wt*	*m*	0.01992	0.03082	0.02572	0.02257
Shoe Thickness	*dsh*	*m*	0.00236	0.00236	0.00236	0.00236
Shoe Taper Length	*dt*	*m*	0.00118	0.00118	0.00118	0.00118
Radius to tooth inner	-	-	0.06739	0.09862	0.084	0.07497
Width of the Tooth Body	*wtb*		0.00443	0.00658	0.00564	0.00479
Width Stator Yoke	*wsy*	*m*	0.00664	0.00987	0.00846	0.00719
Minimum Slot Width			0.01909	0.02785	0.02368	0.02138
Width for 1 set of windings			0.00955	0.01392	0.01184	0.01069
Max winding rows	-	-	8	11	10	9
Winding Radial Rows			2	1	2	2
Windable Slot Depth	*ds*	*m*	0.00473	0.00236	0.00473	0.00473
Slot Area (estimate)	-	*m^2*	9.4E-05	6.7E-05	0.00012	0.0001
Slot Fill Factor	*Kwb*	-	0.41947	0.72272	0.41669	0.50175
Air-gap in Slot	*gs*	*m*	0.00927	0.00691	0.00927	0.00927
Slot Correction Factor	*Ksl*		0.4024	0.47657	0.41051	0.3676
Slot Permeance	*Ps*	*m*	0.51758	0.6657	0.53914	0.43131
Slot Resistance	*Rslot*		0.00558	0.00682	0.00682	0.00744
IR^2 losses	*Pslot*		0.00139	0.0017	0.0017	0.00186
Wire Length	-	*m*	9.87914	15.2371	13.7658	13.9867
wire resistance	*Rwire*	*ohm*	0.00018	0.00028	0.00025	0.00026
Eddy Current Losses	*Pe*	*W*	21.0104	11.3575	17.2572	22.8105
Total Losses			21.0118	11.3592	17.2589	22.8124
Efficiency			91.3992	95.7408	94.0569	92.7923
Motor Constant	*Km*	-	9.05778	16.4455	14.0993	13.0654
Total Mass	-	*kg*	2.39157	3.72808	3.37402	2.72207

REFERENCES

[1] Bianchi, N., Bolognani, S., and Luise, F., 2004, "Potentials and Limits of High-Speed PM Motors", IEEE Transactions on Industry Applications, Vol. 40, No. 6, pp 1570-1578

[2] Brown, D. (2006) "Summer 2006 Electricity Supply and Demand Outlook" *California Energy Commision*, p 26.

[3] Gieras, J., and Wing, M., 2002, *Permanent Magnet Motor Technology: Design and Applications,* Marcel Dekker, New York, NY, pp 43-53, 70, 74

[4] Hanselman, D., 2003, *Brushless Permanent Magnet Motor Design,* The Writers' Collective, Cranston, Rhode Island, pp 7, 29-33, 71-73,109,204-205, 209, 240,252

[5] Hyoung, J. C., Chong, H. A., 2003, "Microscale Resin-Bonded Permanent Magnets for Micro-electrical-mechanial-systems Applications", Journal of Applied Physics, Vol. 93, No. 10,

[6] Jang, S. M., Cho, H. W., Lee, S. H., Yang, H. S., Jeong, Y H., 2004, "The Influence of Magnetization Pattern on the Rotor Losses of High Speed PM Machines", IEEE Transactions on Magnets, Vol. 40, No. 4, pp 2062-2064

[7] Lindberg, B., Papuga, K., Kharazi, A., Mueller, N., 2006, "Novel Compressor Using Woven Composite Impeller", ASME Paper IMECE2006-13342

[8] Mecrow, B. C., Jack, A. G., Atkinson, D. J, Green, S. R., Atkinson, G. J., King, A., Green, B., "Design and Testing of a Four-Phase Fault Tolerant Permanent-Magnet Machine for an Engine Fuel Pump", IEEE Transactions on Energy Conversion, Vol. 19, No 4, pp 671-678

[9] Mueller, N,. Kilikarslan, A, 2005, "A Comparative Study of Water as a Refrigerant with some Current Refrigerants", International Journal of Energy Research,

[10] Ramsden, V. S., Mecrow, B. C., Lovatt, H. C., 1998, "Design of an In-Wheel Motor for a Solar Powered Electric Vehicle.", IEE Proc.-Electr. Power Appl., Vol, 145, No. 5., pp 402-408

[11] Sen, P.C., 1997, *Principles of Electric Machines and Power Electronics,* Wiley, pp 26-30

[12] Xia, Z. P., Zhu, Z. Q., Jewell, G. W., Howe, D., 2003, "Comparison of Halbach Magnetized Brushless Motors equipped with Air-Cored or Iron-Cored Rotors", Journal of Applied Physics, Vol. 93, No. 10, pp 8692-8694,

[13] Zhang, B., Xie C., Hu, J., Wang, H., Gui, Y. H., 2005, "Novel 1-3 Metal Nanoparticle/Polymer Composites induced by Hybrid External Fields", Composites Science and Technology, No. 66, pp

[14] Zhu, Z. Q., Ng, K., Howe, D., 1997, "Design and Analysis of High Speed Brushless Permanent Magnet Motors", Electrical Machines and Drives, 8th International Conference, Publ. No. 444, pp 381-385

[15] Zhu, Z. Q., 2003 , Xia, Z. P., Shi, Y. F., Howe, D., Pride, A., Chen, X. J., "Performance of Halbach Magnetized Brushless AC Motors", IEEE Transactions on Magnetics, Vol. 39, No. 5, pp 2992-2994

[16] Zhu, Z. Q., 2002, Xia, Z. P., Howe, D., "Comparison of Halbach Magnetized Brushless Machines on Discrete Magnet Segments or a Single Magnet Ring.", IEEE Transactions on Magnetics, Vol. 38, No. 5, pp 2997-2999

[17] http://www.matchrockets.com/ether/Halbach.html